

Deep water acoustic range estimation based on an ocean general circulation model: Application to PhilSea10 data

Mengyu Wu, Mikhail P. Barmin, Rex K. Andrew, Peter B. Weichman, Andrew W. White, Eugene M. Lavelly, Matthew A. Dzieciuch, James A. Mercer, Peter F. Worcester, and Michael H. Ritzwoller

Citation: *The Journal of the Acoustical Society of America* **146**, 4754 (2019); doi: 10.1121/1.5138606

View online: <https://doi.org/10.1121/1.5138606>

View Table of Contents: <https://asa.scitation.org/toc/jas/146/6>

Published by the [Acoustical Society of America](#)

ARTICLES YOU MAY BE INTERESTED IN

[Long-range frequency-difference source localization in the Philippine Sea](#)

The Journal of the Acoustical Society of America **146**, 4727 (2019); <https://doi.org/10.1121/1.5138124>

[Source localization in range-dependent and time-varying shallow water: The Shallow Water 2006 experimental results](#)

The Journal of the Acoustical Society of America **146**, 4740 (2019); <https://doi.org/10.1121/1.5138595>

[Convolutional neural network for single-sensor acoustic localization of a transiting broadband source in very shallow water](#)

The Journal of the Acoustical Society of America **146**, 4687 (2019); <https://doi.org/10.1121/1.5138594>

[Bathymetry-aided underwater acoustic localization using a single passive receiver](#)

The Journal of the Acoustical Society of America **146**, 4774 (2019); <https://doi.org/10.1121/1.5138605>

[Bayesian coherent and incoherent matched-field localization and detection in the ocean](#)

The Journal of the Acoustical Society of America **146**, 4812 (2019); <https://doi.org/10.1121/1.5138134>

[Introduction to the Special Issue on Acoustic Source Localization](#)

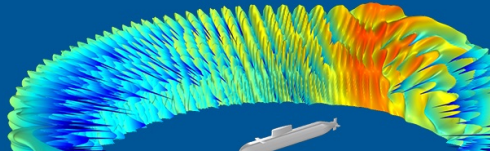
The Journal of the Acoustical Society of America **146**, 4647 (2019); <https://doi.org/10.1121/1.5140997>



COMSOL Day
Acoustics

A free, online event where you can attend multiphysics simulation sessions, ask COMSOL staff your questions, and more

JOIN US MAY 25 »



Deep water acoustic range estimation based on an ocean general circulation model: Application to PhilSea10 data

Mengyu Wu,^{1,a)} Mikhail P. Barmin,¹ Rex K. Andrew,² Peter B. Weichman,³ Andrew W. White,⁴ Eugene M. Lavelly,³ Matthew A. Dzieciuch,⁵ James A. Mercer,² Peter F. Worcester,⁵ and Michael H. Ritzwoller¹

¹Department of Physics, University of Colorado at Boulder, Boulder, Colorado 80309, USA

²Applied Physics Laboratory, University of Washington, Seattle, Washington 98105, USA

³BAE Systems, Burlington, Massachusetts 01803, USA

⁴BAE Systems, Merrimack, New Hampshire 03054, USA

⁵Scripps Institution of Oceanography, University of California at San Diego, La Jolla, California 92093, USA

(Received 14 March 2019; revised 22 July 2019; accepted 23 July 2019; published online 31 December 2019)

This study identifies general characteristics of methods to estimate the absolute range between an acoustic transmitter and a receiver in the deep ocean. The data are from three days of the PhilSea10 experiment with a single fixed transmitter depth (~ 998 m) and 150 receiver depths (~ 210 – 5388 m) of known location, and a great-circle transmitter-receiver distance of ~ 510 km. The proposed ranging methods compare observed acoustic records with synthetic records computed through the HYCOM (hybrid coordinate ocean model) model. More than 8900 transmissions over 3 days characterize the statistical variation of range errors. Reliable ranging methods de-emphasize the parts of the data records least likely to be reproduced by the synthetics, which include arrival amplitudes, the later parts of the acoustic records composed of nearly horizontally launched rays (i.e., the finale), and waves that sample a narrow span of ocean depths. The ranging methods proposed normalize amplitudes, measure travel times, or reject parts of the waveforms beyond a critical time. All deliver reliable range estimates based on the time and path-averaged HYCOM model, although the final method performs best. The principles behind these methods are transportable and expected to provide reliable range estimates in different deep water settings. © 2019 Acoustical Society of America.

<https://doi.org/10.1121/1.5138606>

[KTW]

Pages: 4754–4773

I. INTRODUCTION

Range estimation, which we refer to commonly as “ranging,” is part of the more general location or localization problem, and important as a component of positioning, navigation, and timing (PNT) of underwater platforms, especially when surfacing for position fixes is impractical or undesired (e.g., Dosso, 2003; Richardson and Nolte, 1991; Skarsoulis and Piperakis, 2009; Tan *et al.*, 2011; Tolstoy, 1993; Van Uffelen *et al.*, 2016; Van Uffelen *et al.*, 2013). Various international scientific and governmental organizations deploy undersea vehicles or gliders in sustained monitoring missions for collection of data from the regional and near-shore to the global and deep-ocean environments. Gliders may be deployed autonomously for up to six months or longer for oceanographic data collection. The position of submerged gliders is often poorly known (e.g., Leonard and Bahr, 2016), especially for long mission durations, or when the glider is deployed in an area with strong current or eddy dynamics. Some gliders periodically resurface for Global Positioning System (GPS)-based position fixes or data infiltration or exfiltration. However, intermediate to those times the glider location is uncertain, with uncertainties commonly on the order of kilometers (e.g., Kim *et al.*, 2014; Smith *et al.*, 2010), which is worse for under-ice vehicles that

cannot surface to obtain GPS fixes (e.g., Mikhalevsky *et al.*, 2015). Positional information can be obtained through the use of undersea acoustic ranging, which can be performed passively and with minimal impact on the intended vehicle or sensor platform resources and/or mission. However, methods of long-distance ranging are far from standardized (e.g., Chandrasekhar *et al.*, 2006; Saeed *et al.*, 2019).

Acoustic range estimation is strongly dependent on knowledge of the sound speed characteristics of the ocean, which vary strongly with space and time. There is a fortuitous confluence of increased interest in undersea range estimation with the availability of increasingly advanced, ever higher resolution ocean circulation models. Such models form the foundation for wide-area PNT, which might otherwise need to rely on *in situ* data collection over each new area of operation.

In this study, we ask two principal questions. First, what are the general characteristics of methods that reliably estimate the absolute range between an acoustic transmitter and a receiver for methods based on an ocean general circulation model in a deep water setting? We define “range” as the great-circle horizontal distance between a transmitter and receiver. An “absolute” range estimate provides the actual range between a transmitter and a receiver, in contrast to a “relative” range estimate, which provides the range difference compared to an earlier range estimate. Second, how well does an ocean general circulation model actually perform when

^{a)}Electronic mail: mewu4448@colorado.edu

used as the basis for long-distance absolute acoustic range estimates between an acoustic transmitter and a submerged receiver? Such a general circulation model will be most useful in regions where directly measured *in situ* sound speed measurements are rare or absent.

To address these questions, we present and assess four methods of absolute acoustic ranging, all based on the comparison between observed and synthetic acoustic waveforms. We compute synthetic acoustic waveforms using an adiabatic normal mode code of our own construction. The first method (method 0), a direct cross correlation between the synthetic and data records, is the most straightforward way to compare observed and synthetic records. However, as we will show in Sec. IV B, it does not provide reliable range estimates. In response, we also present three refined ranging methods, methods 1–3, that aim to address the shortcomings of method 0 in different ways. Each defines a different approach to ranging either by normalizing amplitudes (method 1), measuring travel times (method 2), or rejecting the parts of the waveforms later than a critical time (method 3). Throughout the paper, we refer to these as methods 0–3, and Table I summarizes them for reference. We test the ability of each of the methods to deliver reliable range estimates, where we define reliability in terms of bias (or systematic error), fluctuation, outlier production, and sensitivity to errors in the ocean model.

To assess these ranging methods we employ one of the members of the HYCOM (hybrid coordinate ocean model, e.g., Chassagnet *et al.*, 2007) family of models and the acoustic data set collected in the Philippine Sea by the University of Washington from 8 to 10 May 2010 (Andrew *et al.*, 2016; Andrew *et al.*, 2010), which was part of a multi-institution experiment that we refer to as the “PhilSea10” experiment (e.g., Worcester *et al.*, 2013). The locations of the transmitter and receiver arrays are placed in a regional context in Fig. 1.

The HYCOM model we use (GOFS 3.0, GLBa0.08) is a daily averaged model that began in September 2008, and also assimilates ocean property data from satellite and *in situ* measurements. The horizontal resolution is about 0.08° , and there are 33 layers with depth. We convert the model to sound speed by applying routines from the Gibbs Seawater (GSW) toolbox (McDougall and Barker, 2011) and interpolate onto a 1 m depth grid. Our computations are typically performed on the three-day average of this HYCOM model for May 8–10, 2010. In addition, range estimates are presented for the path-averaged model between transmitter and receiver. For simplicity, we refer to each of these models of sound speed (the input model, the time-averaged model, and the additionally range-averaged model) as the “HYCOM model” or sometimes just “HYCOM.” Context will determine which of these variants is meant. Figure 1 displays the

sound speed field for the HYCOM model at several depths in the region around the transmitter (star) and receiver (diamond), illustrating the length scales of resolved ocean acoustic features. Variations homogenize at greater depths. Figure 2(a) presents the sound speed profile averaged along the path between the transmitter and receiver array. As Fig. 2(b) illustrates, the HYCOM model undergoes significant temporal variations (up to 0.2%, which is much larger than our range error below) during the month of May, but they are largely confined to the top 500 m of the ocean.

For the PhilSea10 data we use here, the acoustic transmitter was set at $19^\circ 00'N$, $130^\circ 12'E$ at a depth of about 998 m (Fig. 1). The transmitter was driven by an M-sequence signal (e.g., Munk *et al.*, 2009; Worcester *et al.*, 1985), which repeats every 20.46 s. We use about 8900 transmissions (sequence periods or pings) over 54 h in our tests, which presents a large database to study the effect of ocean state variations on range estimates. The acoustic signal was observed with a distributed vertical line array (DVLA) composed of 150 hydrophones. This DVLA was deployed nominally at $21^\circ 21.7418'N$ and $126^\circ 0.7867'E$ with nominal hydrophone depths from about 180 to 5381 m (Andrew *et al.*, 2016). The mooring motion of the DVLA was tracked once per hour, and the real position of each hydrophone changes somewhat with time during the experiment in a known way. The DVLA allows tests of the ranging ability over a wide set of receiver depths.

A beneficial characteristic of the PhilSea10 data set is that transmitter and receiver locations are tracked and approximately fixed, and we consider them to be the ground truth. Therefore, range estimates can be converted to range errors and the statistical distributions of the errors studied. We consider a reliable absolute range estimator to have a bias (or systematic error) smaller than approximately 20 m, a Gaussian fluctuation of no more than about 20 m, with fewer than about 10% of estimates in error by more than 200 m. A 20 m error at 500 km separation (four parts in 10^5) is a significant achievement, corresponding to only ~ 6 cm/s path-averaged model sound speed error. Average ocean currents were weak (< 1 cm/s) during the PhilSea10 experiment as estimated by the HYCOM model, and will be ignored in the following.

We discuss the data set and synthetic methodology used in this study in Secs. II and III. Section IV presents the four ranging methods and the statistics of their performance based on the HYCOM model. Section V discusses the characteristics of the ranging methods that are needed to deliver reliable absolute range estimates, discusses sources of bias and fluctuation, and considers the resolution and relative merits of the refined ranging methods (methods 1–3).

TABLE I. Four methods to estimate range.

Method	Description
Method 0	Direct cross correlation between synthetic and observed records to estimate range
Method 1	Convert synthetic and observed records to telegraphic signals, then cross correlate to estimate range
Method 2	Measure travel times of peaks on synthetic and observed records, optimal agreement between the sets of peak times provides the range estimate
Method 3	Reject segments of the synthetic and observed records later than a critical time (finale), then cross correlate to estimate the range

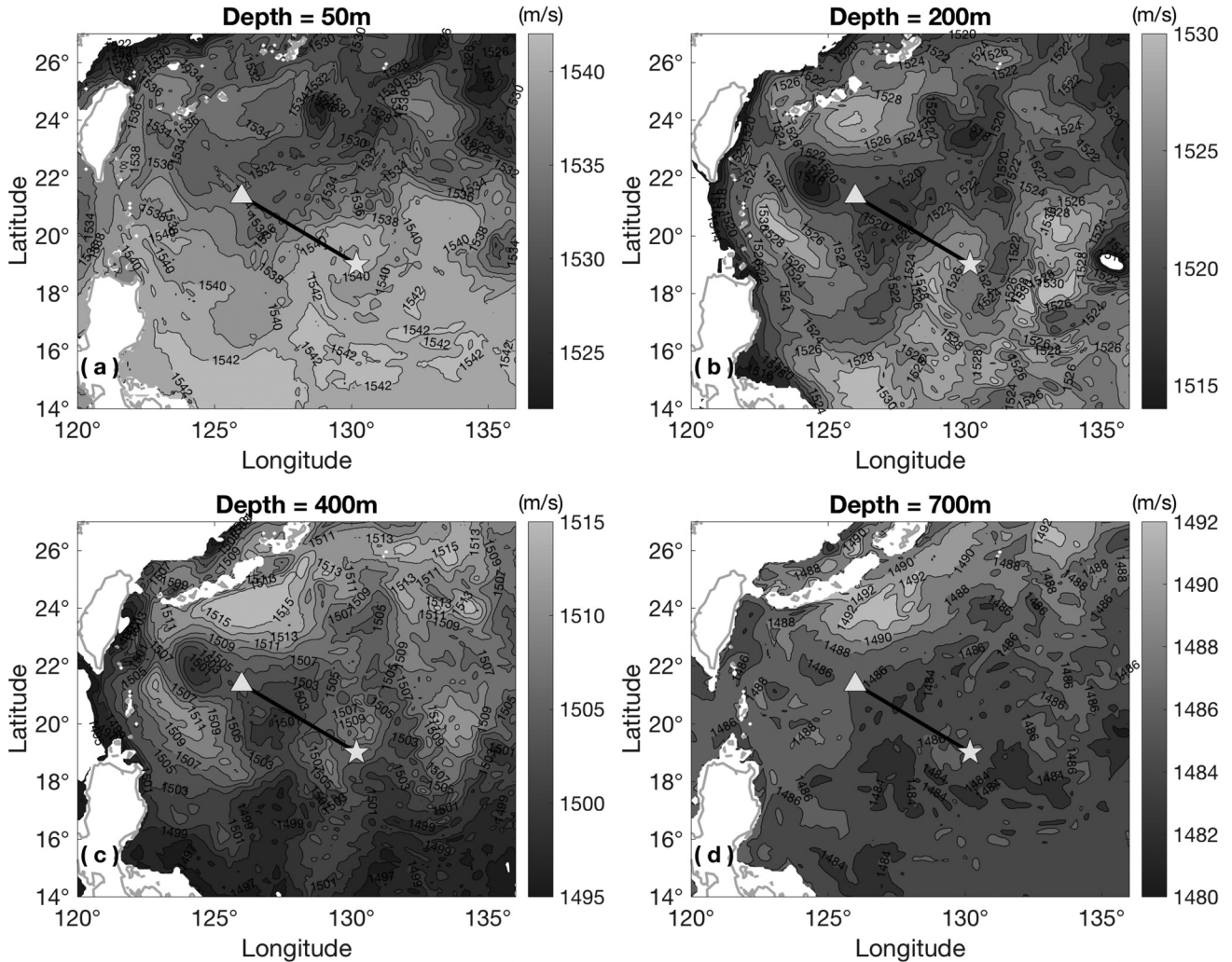


FIG. 1. Horizontal slices of acoustic wave speeds from the HYCOM model (three day mean from May 8 to May 10 2010) at depths of about (a) 50 m, (b) 200 m, (c) 400 m, and (d) 700 m. The deeper slices are nearly homogeneous and not shown here.

II. DATA

The signal that drives the acoustic transmitter in the PhilSea10 data set is a known M-sequence with both 200 and 300 Hz sinusoid carrier waves. The signal that is actually transmitted, $s(\omega)$, is not as well known, however, and differs appreciably from the drive signal. To deal with this, the experimenters installed a “monitor” hydrophone at about 20 m from the transmitter, and we use the Fourier transform of the signal recorded at the monitor hydrophone,

$$s(\omega) = S(\omega)e^{i\psi(\omega)}, \quad (1)$$

as a preliminary model of the radiated signal, where the magnitude and phase S and ψ , respectively, are real-valued functions of frequency, ω . We smooth $S(\omega)$ prior to using it. Figure 3(a) presents an example of the smoothed radiated signal spectrum observed at the monitor hydrophone for a single ping. The radiated signal spectrum lies predominantly in two discrete frequency bands. Because of its higher spectral amplitude, we focus on the lower frequency band by applying a real-valued Gaussian window function, $G(\omega)$, with mean of 212 Hz and standard deviation of 12 Hz. The resulting spectral model for the radiated signal is shown in Fig. 3(b).

The $d \sim 20$ m offset between the transmitter and the monitor hydrophone produces a small phase shift $\sim \omega d/c$ that we correct in the model of the radiated signal, so that $\psi(\omega) \rightarrow \tilde{\psi}(\omega)$. Thus, our model of the radiated signal becomes

$$\tilde{s}(\omega) = G(\omega)S(\omega)e^{i\tilde{\psi}(\omega)}. \quad (2)$$

Errors in our knowledge of the exact location of the monitor hydrophone and exact sound speed in the neighborhood of the transmitter will degrade our knowledge of the radiated signal in detail, and may produce range errors of up to several meters.

Each ping in the M-sequence is 20.4600 s in duration, and more than 160 pings are transmitted each hour. The transmitter is typically quiet for several minutes before the end of each 1-h segment and begins again at the beginning of the next 1-h segment. In total, we use observations from more than 8900 pings covering 54 h.

We time-compress the raw observed acoustic records for each ping at each array depth by “phase-only filtering.” For ping i and receiver depth z_j , where $z_j \in [210 \text{ m}, 5388 \text{ m}]$ and $1 \leq j \leq 150$, let the recorded acoustic record in the frequency domain be written

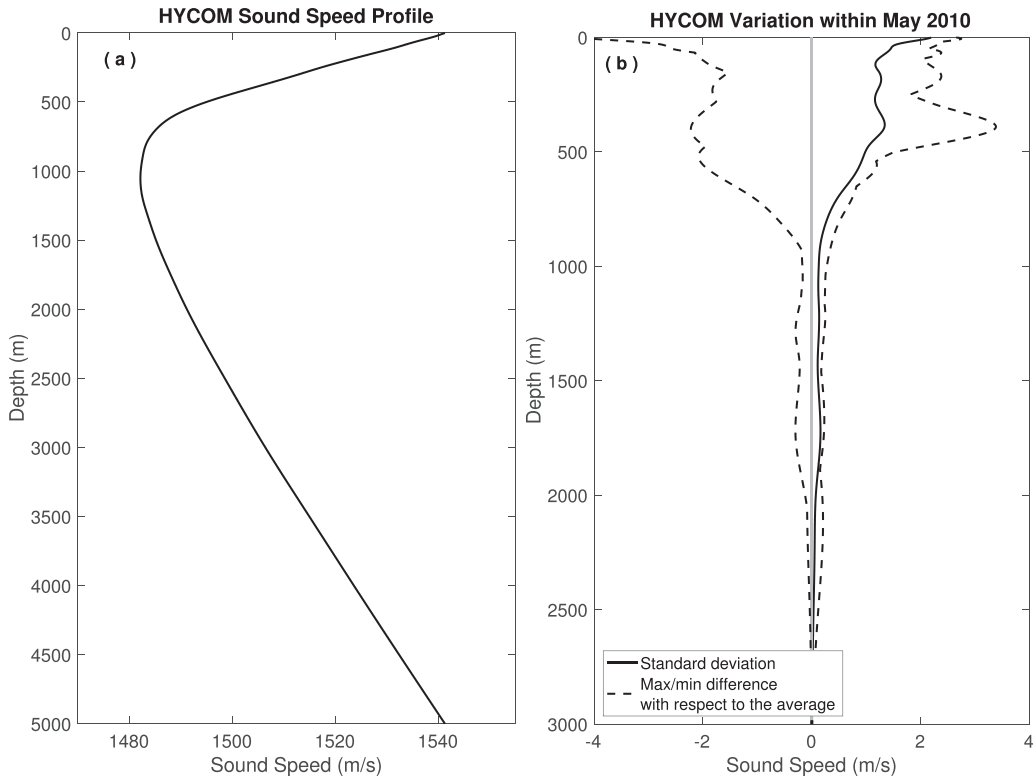


FIG. 2. (a) Path-averaged sound speed profile from the transmitter ship to the receiver array for the HYCOM model (three-day mean, May 8–10 2010). (b) The variability of the path-averaged HYCOM sound speed model during May 2010. Standard deviation of acoustic wave speed of daily averages over the month (black line). The maximum and minimum of the daily values during the month compared with the monthly mean (dashed lines).

$$r_{ij}(\omega) = R_{ij}(\omega)e^{i\phi_{ij}(\omega)}, \quad (3)$$

where R and ϕ are the real-valued amplitude and phase spectra of the observations. In this study, time compression involves deconvolving only the phase part of the radiated signal ($\tilde{\psi}$) from each observed record

$$d_{ij}(\omega) = G(\omega)R_{ij}(\omega)e^{i[\phi_{ij}(\omega)-\tilde{\psi}(\omega)]}, \quad (4)$$

where $G(\omega)$ is the Gaussian sampling function applied to the radiated signal spectrum in order to accentuate the low frequency

signal. Thus, $d_{ij}(\omega)$ defines the time-compressed observed signal for ping i and depth z_j , which we convert to the time domain for further analysis: $d_{ij}(t)$. Here, we present only the envelope of compressed time-domain records in which the observed carrier wave (near 212 Hz) is suppressed.

Examples of time-compressed acoustic records following a single ping are shown in Fig. 4(a). The acoustic waveforms are quite well observed to a depth of about 4700 m for each ping, although the relative amplitude of the peaks, the number of peaks, and, to a lesser extent, their timing differ between pings.

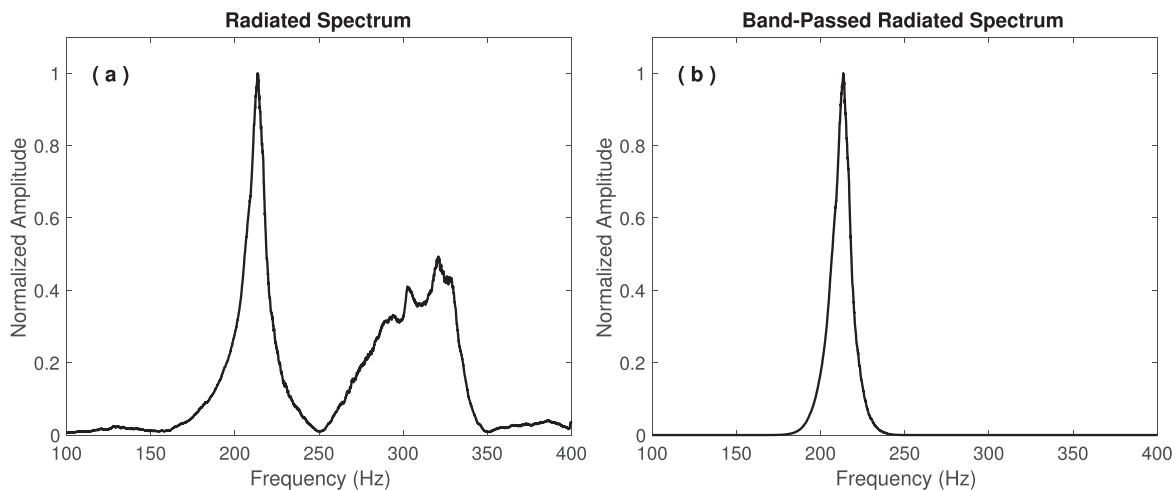


FIG. 3. (a) The radiated spectrum $S(\omega)$ for a single ping taken from a nearby monitor hydrophone, illustrating the frequency content of the radiated signal. (b) The band-passed model spectrum, $G(\omega)S(\omega)$, which identifies the frequency band of our emphasis, where $G(\omega)$ is a Gaussian with a mean of 212 Hz and standard deviation of 12 Hz.

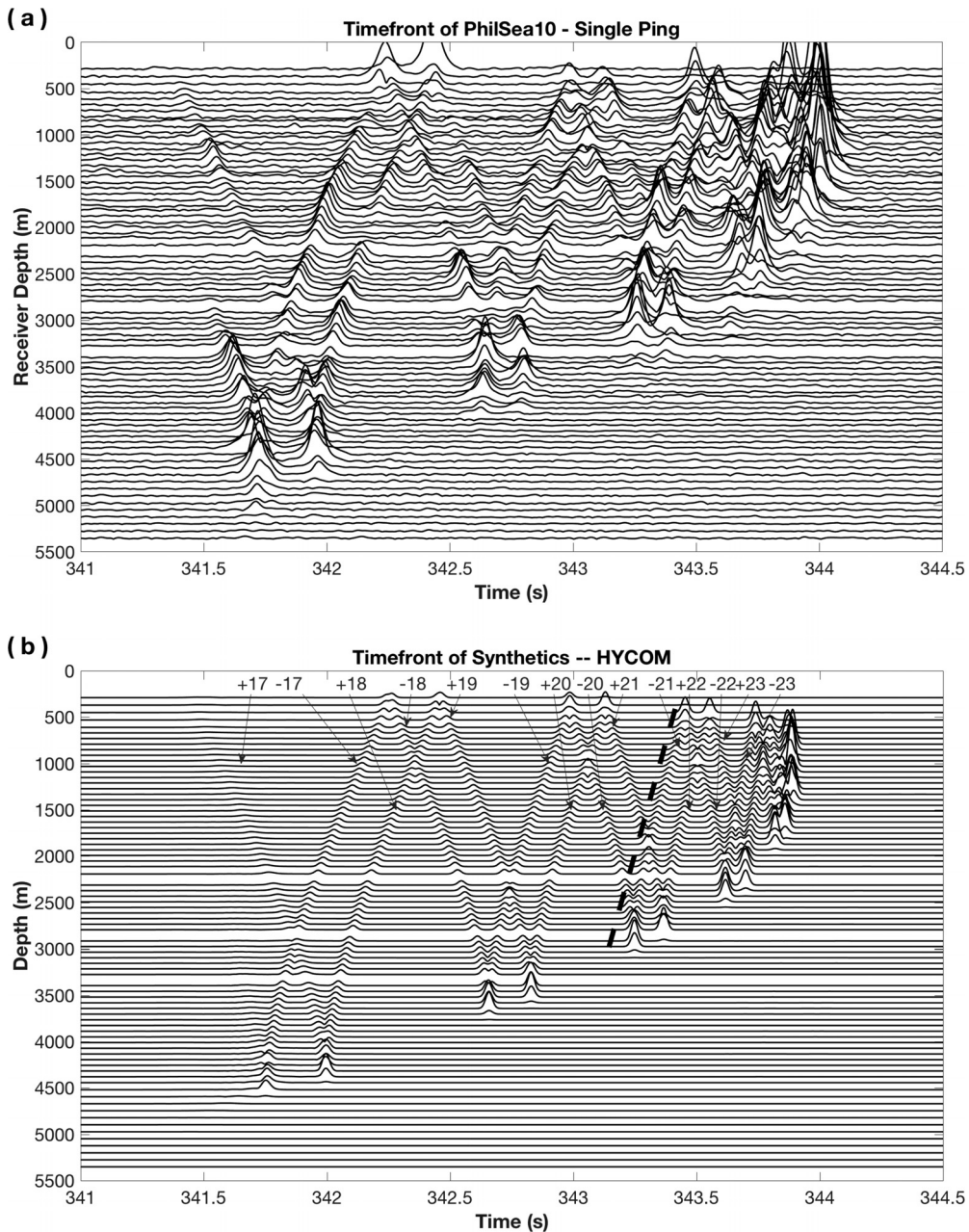


FIG. 4. Examples of envelopes of the observed and synthetic time-fronts, presented at selected array depths. (a) Observed time-front for a single ping. The receivers near the deep sound channel and bottom are set more densely, and some of them are not shown here. The three gaps near 2200, 2800 and 3400 m are real; no receivers are set there. (b) The synthetic time-front computed through the path-averaged HYCOM model [Fig. 2(a)] using the average transmitter-receiver distance at depths comparable to the observed time-fronts in (a). Ray identifiers (IDs) are indicated and the bold black dashed line defines the onset of what we call the “finale.”

To present an estimate of range error, the transmitter and the receiver array locations must be known as the ground truth. The transmitter was suspended from the ship R/V Roger Revelle, which kept a stable position dynamically during the experiment. The experimenters monitored the drift of the transmitter using a long-baseline acoustic navigation system, which shows that the time-variable uncertainty of the transmitter location is within a couple of meters compared to the nominal position ([Andrew et al., 2016](#)). Thus, we will assume that the transmitter location is known and fixed during the experiment, with an uncertainty of a few meters, and also the transmitter depth of 998 m is fixed.

The receivers were divided by the experimenters into five subarrays, and the locations of the controllers in each subarray were tracked by a long-baseline acoustic navigation system once per hour during the entire PhilSea10 experiment. We estimate the horizontal position of the hydrophones by linear interpolation between the depth of controllers and between the hours of observation. In the PhilSea10 data set, the northing and easting offsets of the hydrophones from their mean values are on the order of tens of meters. We assume that the time-variable horizontal location of each receiver is known, but, in fact, horizontal positions have an accuracy of ~ 1 m root-mean-square (rms).

In addition, we assume that the depth of each receiver is fixed with time, but, in fact, it does vary by several meters, positive and negative. Above about 2400 m, receiver depth varies predominantly semi-diurnally within ± 2 m with a few exceptions. Below this depth, variations are more nearly hourly, and amplitudes (again, with a few exceptions) lie within ± 7 m. Because perturbing receiver depth changes the time of arrival of some data peaks positively and others negatively, there is an offsetting effect on range estimates, except for arrivals in the finale which have travel time shifts in the same direction that do not compensate each other. Therefore, the range error caused by unmodeled perturbations in receiver depths is negligible for methods 1–3, which de-emphasize the finale. Receiver depth variations will contribute larger range errors for method 0, but will probably only produce fluctuations at a magnitude of a few meters.

The speed of the drift of the array is less than about 10 m/h at all depths. This rate of motion is small enough that it is unnecessary to apply a Doppler correction to the phase of the recorded signals. Ignoring this correction will contribute a range error of less than 1 m, which will vary over time as the magnitude and sign of the velocity of the array components change.

III. SYNTHETIC WAVEFORMS

Many methods (e.g., wavenumber integration, normal modes, and parabolic equations) are commonly used to compute synthetic wavefields through a given ocean acoustic model (Colosi and Morozov, 2009; Flatté and Vera, 2003; Jensen *et al.*, 2011; Schmidt and Kuperman, 1995). Here, we use an adiabatic normal mode method (e.g., Jensen *et al.*, 2011) to calculate synthetic waveforms for ranging. We refer to our code by the name NMPP, which stands for “normal mode phase propagation.”

NMPP is intrinsically two-dimensional (2D), there are no three-dimensional (3D) effects so that waves propagate in the vertical plane linking the transmitter and receiver. The method is adiabatic; that is, there is no modal coupling, and we apply pressure-release boundary conditions at both the surface and bottom of the ocean. A pressure-release bottom boundary is acceptable because water depth is great enough so that there are no bottom-interacting arrivals. The eigenvectors vanish below 4500 m depth before reaching the bottom. The theory is Cartesian, but we apply an earth-flattening transformation (e.g., Chapman, 1973) to approximate wave propagation in a spherical oceanic shell and accumulate distances and determine great-circles on the oblate spheroid (Karney, 2013). Modes are retained from modal indices of 1–250 at frequencies ranging from 162 to 262 Hz, we perform computations in the frequency domain on an intrinsic frequency grid of 0.5 Hz, and then results are interpolated to a grid spacing of 0.01 Hz.

Synthetic waveforms are computed based on the HYCOM acoustic model between the transmitter and receiver locations shown in Fig. 1, where the HYCOM model is the three-day average from May 8 to May 10, 2010, interpolated on to a 1 m vertical grid.

We tested the importance of including range dependence in the synthetics by comparing the range-dependent synthetics (with 20 intermediate points between transmitter

and receiver) to range-independent synthetics using several different sound speed profiles from the Philippine Sea. We find that the range-dependent synthetics are quite similar to the range-independent synthetics using the profile averaged along the path (path-averaged profile) with a maximum time offset of arrivals of about 4.5 ms. This is not surprising because the adiabatic approximation integrates the slowness of each mode, similar to the path-average profile. This time offset would correspond to a maximum range error of about 7 m. We use the path-averaged model to compute range-independent synthetics in this study, which has the side benefit of substantially increasing numerical efficiency.

The use of range independence may fail to produce synthetics of sufficient accuracy in ocean regions with greater horizontal variability. Over longer ranges, 3D effects, such as horizontal refraction and horizontal multipath propagation, could also become more significant. As discussed later, the PhilSea10 data set is rather ideal in this sense (although there is strong eddy activity in the Philippine Sea outside the PhilSea10 experiment), but this has the advantage of allowing us to focus on the specific basic questions outlined in the Introduction with minimal additional complication. Future studies can then broaden the scope.

To define the range-independent path-averaged model at each depth we compute the average acoustic slowness along the great-circle linking transmitter and receiver. There is a subtlety here due to topography on the sea floor. To determine the range-independent model, we set the ocean depth to the maximum sea floor depth between transmitter and receiver, which is about 5500 m for the HYCOM model. For water depths above the minimum sea floor depth between the transmitter and receiver, all locations on a 5-km-spaced grid between transmitter and receiver are used to average the acoustic slowness. However, to find the average acoustic speed at a water depth between the minimum and maximum sea floor depths, only those grid locations where the seafloor depth is greater than the water depth are used to compute the average.

We anticipate greater acoustic scattering near the surface and sea floor. To attenuate waves that sample right near the sea surface and ocean bottom, we apply a “quality factor” or Q model (Jensen *et al.*, 2011) that is equal to 10 000 at the surface and increases linearly to 300 000 at a depth of 500 m. The model similarly decreases from 300 000 to 10 000 linearly as depth increases from 4800 to 5300 m. Between depths of 500 and 4800 m, Q is 300 000, and at depths greater than 5300 m, Q is 10 000. This Q model has only a small effect on the synthetics.

For depth z_j , let the resulting synthetic waveform computed in the frequency domain be denoted $u_j(\omega)$. To provide better agreement with the data, we multiply by the same Gaussian sampling function as applied to the data [Eq. (4)] so that the band limited synthetic becomes

$$\tilde{u}_j(\omega) = G(\omega)u_j(\omega), \quad (5)$$

where, again, $G(\omega)$ has a mean value of 212 Hz and a standard deviation of 12 Hz. As discussed later, when we compare synthetics to data we will additionally multiply by the radiated signal spectrum, $S(\omega)$.

An example of a synthetic time-front diagram, computed by applying NMPP to the path-averaged HYCOM model, is shown in Fig. 4(b) where the acoustic speed profile is presented in Fig. 2(a). The path-averaged sound speed profile is typical for such profiles at mid-latitudes: relatively high speeds near the surface and deep in the ocean with a low velocity zone at central depths forming the deep sound channel. Parallel arrivals begin to appear in the time-front diagram at about 341.7 s, similar to the data [Fig. 4(a)]. The parallel pairs of earlier arrivals may be interpreted as pairs of conventional rays that are launched steeply from the transmitter at both positive and negative angles. Ray identifiers (IDs), which indicate the sign of the launch angle (positive means the ray goes up initially) and the total number of turning points of the ray path, are also indicated in Fig. 4(b). The peaks at times earlier than 341.7 s do not appear as clearly in the synthetics as in the data [Fig. 4(a)]. To resolve them properly would require retaining more than 250 modes (i.e., including those with eigenfunctions that span a greater range of vertical distances from the channel axis) and the use of a vertical grid smaller than 1 m.

IV. RANGING METHODOLOGY AND RESULTS

We investigate the “range inverse problem,” which is to determine the horizontal distance between a given transmitter and a given receiver. For each transmitter-receiver pair, this involves determining a single range estimate, which varies with time as each successive transmission (ping) is received. Because the PhilSea10 data set contains ground truth information about the transmitter and receiver positions, we present the results of our inversion experiments in terms of “range error” rather than range.

We do not explore the “location or localization inverse problem” (e.g., [Van Uffelen et al., 2016](#)), although this is a natural extension of our investigation. Location estimates are triples of numbers, e.g., (x,y,z) for each receiver. However, receiver depth, z , can be estimated from *in situ* pressure, which reduces the location inverse problem to the estimation of two quantities. These quantities, (x,y) , can be determined from range estimates between a receiver and a number of transmitters at different locations using a wide variety of triangulation methods ([Freeman et al., 2015](#)). The location inverse problem can be formulated as a series of range estimates, although not all location methods take this approach ([Zhebel and Eisner, 2015](#)).

The unifying idea that underlies the ranging methods we discuss and test is the comparison of observed and synthetic recordings. Our approach is to try to minimize the difference between an observed waveform, $d(t)$, and a synthetic waveform computed through an ocean model, $u(t)$. In practice, the synthetic waveform is computed using an initial range estimate, R_0 , and we seek to find the shift in time, δt , that will bring the observed and synthetic records into optimal agreement in some sense. The effective shift in range, δR , can be computed from the time shift, $\delta R \approx c\delta t$, where we use $c = 1480$ m/s to convert between the time and range shifts. In this case, the range estimate is $R = R_0 + \delta R$. We seek to identify a ranging method or methods that will minimize the

absolute value of the range error, R_{err} , such that $R_{\text{err}} = R_{\text{GT}} - R$, where R_{GT} is the ground truth range. We discuss the dependence of the ranging methods on the initial range estimate, R_0 , in Sec. IV D.

We present and discuss four ranging methods (methods 0–3) based on different notions of optimality concerning the alignment of the data and synthetic records. The first method (method 0) is the direct cross correlation between the synthetic and data records. This method does not work well at most depths due to its attempt to align the largest amplitude peaks in the data and synthetics, which may be for different arrivals in the two records or may be in the finale of the record. The finale is the part of the observed waveforms that is most poorly predicted by the synthetics. Therefore, we also present three refined methods, methods 1–3, that aim to down-weight in different ways the largest amplitude peaks and/or the later arrivals either by normalizing amplitudes (method 1), using measured travel times (method 2), or rejecting the parts of the waveforms later than a critical time (method 3) in order to downplay the effect of the finale. Each of these methods performs, on average, better than method 0, but there are depths at which each method performs in less than an ideal way. In principle, each method could be iterated repeatedly, but here we present only the first iteration.

The fidelity of the ocean model is an important factor to determine whether synthetics and observations agree well enough so that their comparison can be used as a basis for ranging. Significant investments have been made in the development of ocean models, assimilating all available high quality data and being as true as possible to the physics of the underlying fluid equations. Any ocean model will be inaccurate at some level, and accuracy of long-distance range estimation provides a significant test of such models ([Dushaw et al., 2009](#)). Therefore, we also seek to produce ranging methods that are relatively insensitive to errors in the ocean model. Model infidelity will vary with depth and choice of time of the acoustic record. Recognizing this, methods 0–3 provide varying degrees of robustness depending on the nature of the errors in the sound speed profile. As such, no single method can be universally applicable, but our study provides some selection guidance (summarized in the Conclusions).

A. Preliminary comparison between synthetic and observed waveforms

Comparisons between broadband acoustic data and synthetics (or travel times) are actually rare in the open literature. Exceptions include [Howe et al. \(1987\)](#), [Worcester et al. \(1994\)](#), [Colosi et al. \(1999\)](#), [Worcester et al. \(1999\)](#), and [Andrew et al. \(2016\)](#).

In comparing synthetics to data, we modify the band limited synthetics $\tilde{u}(\omega)$ of Eq. (5) by multiplying by the radiated signal spectrum in the frequency domain [Fig. 3(b)]

$$\tilde{\tilde{u}}_j(\omega) = S(\omega)\tilde{u}_j(\omega). \quad (6)$$

This is necessary because the true radiated signal spectrum is actually narrower than the Gaussian sampling function—see Figs. 3(a) and 3(b)—so that data peaks in the time

domain are broader and tend to overlap one another more than synthetics computed without the true radiated spectrum. Figure 5, for example, illustrates how the resulting peak widths of the synthetics shaped by the radiated signal spectrum match those of the data. We use the envelope of $\tilde{u}(t)$ to compare to the envelope of the data, $d(t)$, in the remainder of this paper. The resulting synthetics and data are sufficiently broadband to obtain usable waveforms and travel times for range estimates (e.g., Duda *et al.*, 2006).

To provide a preliminary comparison between observations and synthetics, we stack observed waveforms from ~ 160 pings over one hour to provide higher signal-to-noise ratio (SNR) waveforms than those in Fig. 4(a) to compare with synthetics. Figure 5 overplots these stacked observed waveforms at seven receiver depths with synthetics computed through the path-averaged HYCOM model. The synthetics display a similar set of arrival peaks as the data [as Figs. 4(a) and 4(b) also show]. However, the peaks in the synthetics tend to come in a little later than observations for the early arrivals, and then the time difference gradually decreases in the middle of the waveform and reverses for the latest arrivals. Thus, although the HYCOM model appears to be a bit slow for the entire ocean column, which the earliest arrivals sample, it is too fast in the deep sound speed channel, which dominates the finale for the time period of this experiment. In addition, the relative amplitudes between the synthetics and the observations do not agree well in detail. Notably, the finale, at depths where it

exists, is the part of the observed records most poorly reproduced by synthetics.

Comparisons between observed and synthetic records, such as those shown in Fig. 5, are encouraging and have helped to motivate this study. The details of the differences between the observed and synthetic records will determine whether a given ranging method will deliver an accurate range estimate, may be biased systematically, or may be prone to generate outliers. We can understand these biases in some detail in terms of the sensitivity of different modes to different ocean depth ranges. It would be interesting to verify these conclusions in cases where coincident *in situ* measured sound speed profiles were available, but this lies beyond the scope of this paper.

B. Initial ranging method (method 0, M0)—Direct cross correlation

Comparisons of observed and synthetic waveforms, such as those shown in Fig. 5, motivate a ranging method based on the direct comparison between the two waveforms. As a start, we introduce a particularly simple initial technique, method 0 (M0), which is based on a comparison between synthetic and observed acoustic traces directly by cross correlation. The peak of the cross correlation defines the time shift, δt , between the synthetic and observed records, which we translate to a shift in range, δR , and then compare the resulting range estimate with the ground truth range to estimate the range error, R_{err} .

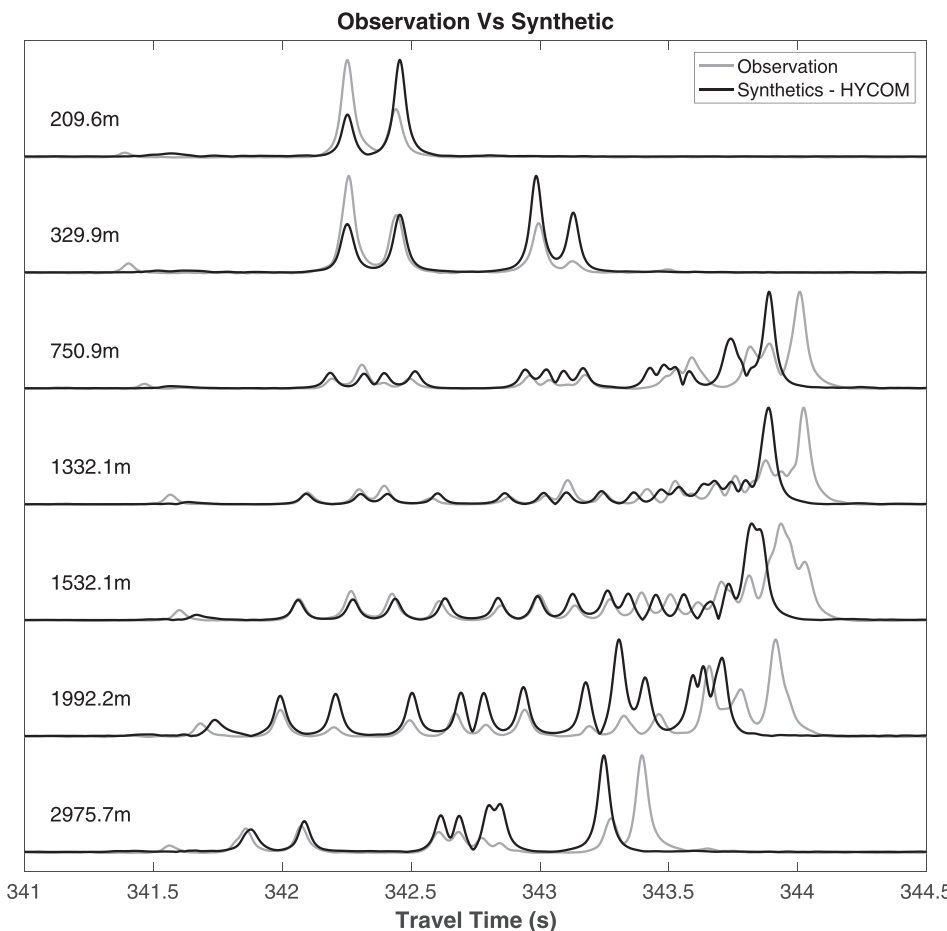


FIG. 5. Envelopes at seven depths of synthetic waveforms computed through the path-averaged HYCOM model (black lines) over-plotted with the observed waveforms (grey lines), which are a stack of all pings over one hour to improve the signal-to-noise ratio (SNR). The ground-truth range has been used to compute the synthetics. Synthetic arrivals are usually late for the earliest peaks, on time for the middle peaks, and early in the finale.

Figure 6 presents examples of cross correlations using synthetics computed for a single ping, with receivers at depths of approximately 330 and 2976 m. At 330 m depth, the correlation peak in Fig. 6(c) appears at a time lag between the observed and synthetic records of less than 2 ms, or approximately a range error of -2 m relative to the ground truth. This small error results despite the fact that the synthetic and observed records display a different number of arrival peaks. In effect, the cross correlation attempts to align the largest amplitude peaks, which, in this case, results in a small range error. Side peaks in the cross correlation identify other alignments that deliver a fairly good correlation between the two signals as the synthetic is slid past the observation. The existence of side peaks is one of the major problems facing this (and probably any) ranging method based on the comparison of observed and synthetic waveforms: the method of alignment of the synthetic and observed records may be confused by discrepancies between the records and produce a number of peaks in the cross correlation. In some cases, range estimates could be based on the wrong peak in the cross correlation, which would result in bi- or multi-modal range error distributions. Such confusion is evident in Figs. 6(d)–6(f) for a depth of 2976 m. At this depth the cross correlation does not perform well

because the largest amplitudes are in the finale of the observed signal, which is poorly fit by the synthetic. This produces an apparent time shift relative to the ground truth of about 167 ms for this ping or a range error of 247 m.

Figure 7 presents summary histograms of range errors, or range error distributions, at six receiver depths spanning from 210 to 2976 m for M0. To produce Fig. 7, we use the continuous 54-h data set of 8910 pings and estimate the range error of each ping individually for all receivers in the array. We present statistics only for those pings with $\text{SNR} > 10$, where we define SNR as the ratio of peak amplitude to the rms of the trailing noise (after the finale). This reduces the number of pings to somewhat more than 7000 at most depths. Each new ping provides a repeated range estimate. As discussed later, we believe that variations in range estimates over time will result primarily from how changes in ocean state affect the travel time and amplitude structure of the observed waveforms.

For M0, range error distributions are often bi- or multi-modal. The mean and standard deviation of range errors, therefore, do not provide representative summaries of the likelihood of a reliable range measurement or the tendency for the method to fail. We find that more useful summary statistics are given by three numbers: (1) the mean (μ) and

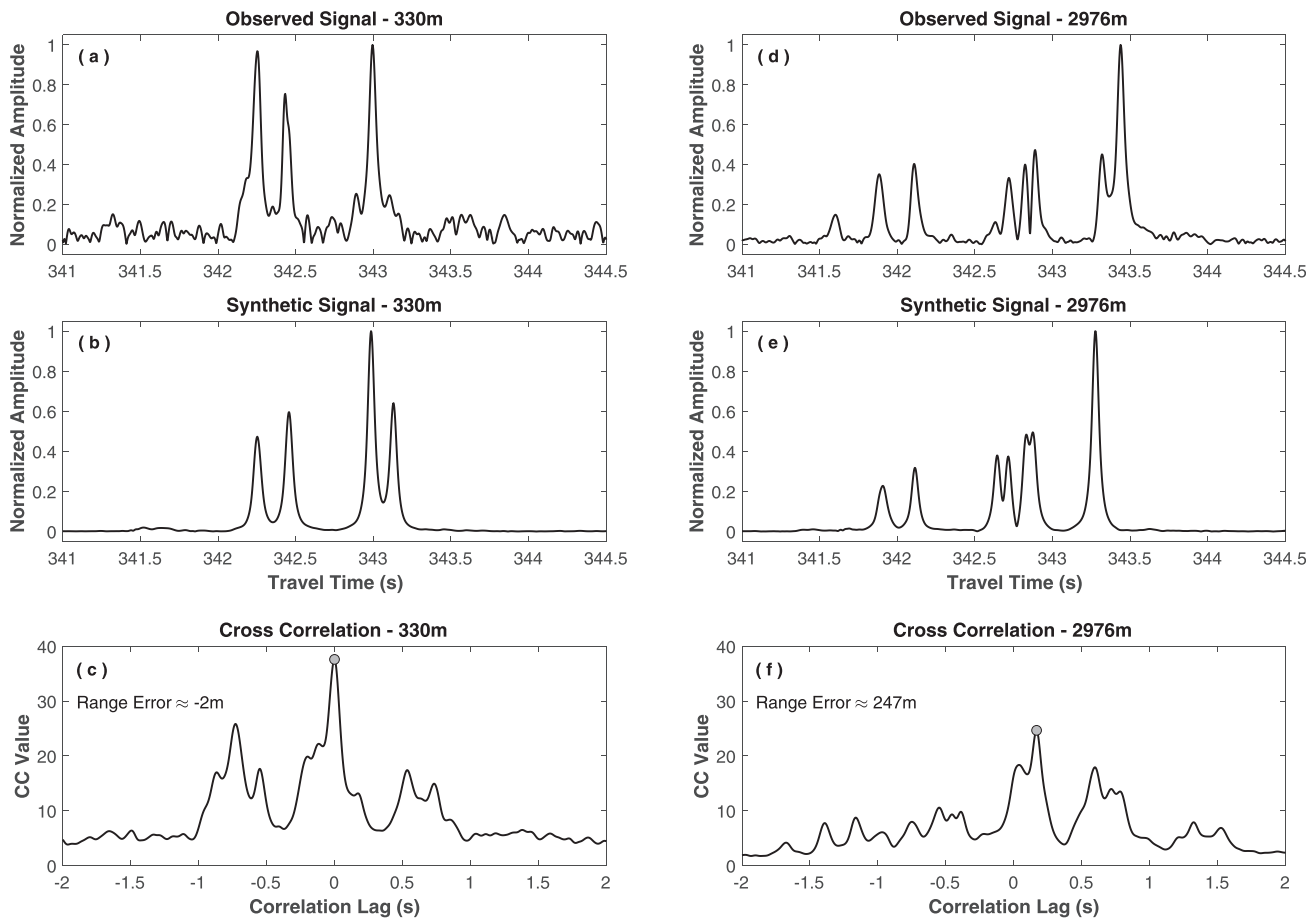


FIG. 6. Illustration of the result of applying M0 to data from a single ping: direct cross correlation between the observed and synthetic records. (Left column) Receiver at a depth of ~ 330 m. (Right column) Receiver at ~ 2976 m depth. (Top row) Observed records for the ping. (Middle row) Synthetics computed for the receiver depth using the ground truth range. (Bottom row) Cross correlation of the observed and synthetic signals, in which the time axis represents a shift relative to the ground-truth location. Positive correlation lags are shifts in time consistent with moving the receiver away from the transmitter, which results when the ocean model is too fast. The range errors are listed in (c) and (f).

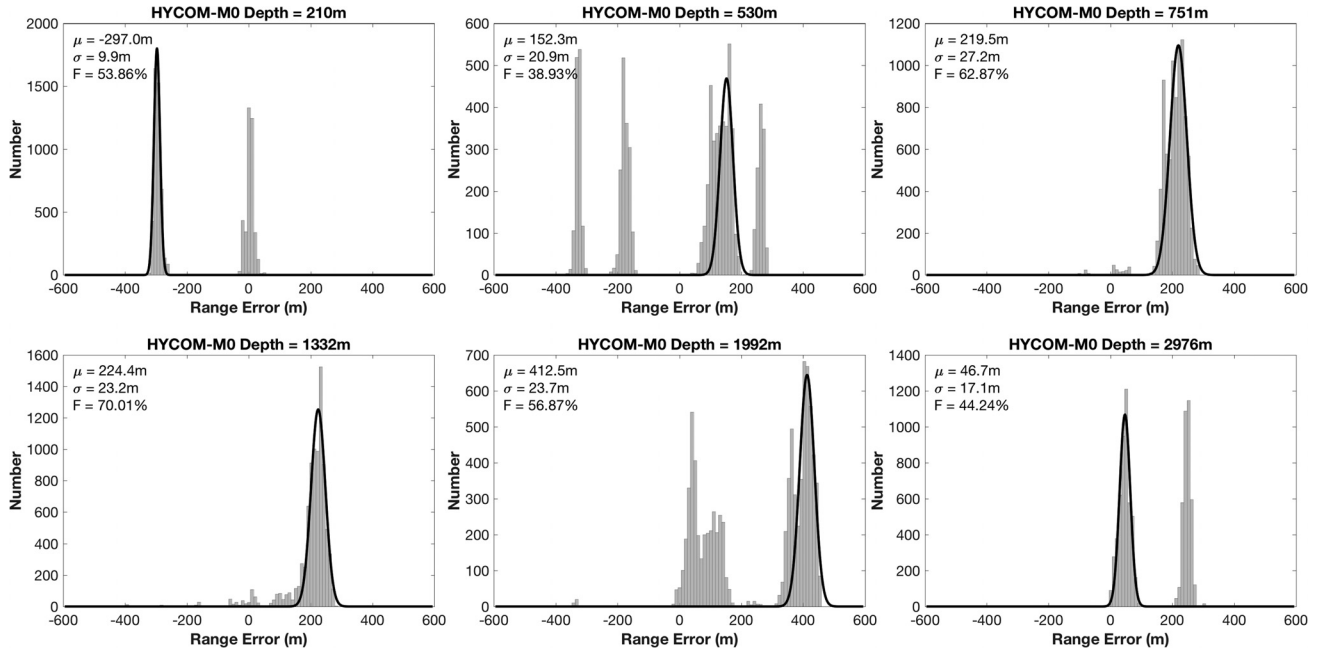


FIG. 7. Histogram of range errors from M0 based on 8910 pings at 6 receiver depths, using the HYCOM model. Zero error indicates the range estimate is equal to the ground truth range. Statistics on each subfigure include the bias (μ), fluctuation (σ), and percentage of outliers whose error is greater than 200 m (F). Positive errors indicate the receiver is located too far from the transmitter, which results when the ocean model is too fast. Black lines are the Gaussian functions $[N(\mu, \sigma)]$ fit to the largest amplitude lobe in the error distribution.

(2) standard deviation (σ) of the Gaussian fit to the largest amplitude peak or mode of the error distribution, and (3) the fraction (F) of range estimates in error by more than 200 m. The fit Gaussian $[N(\mu, \sigma)]$ is found by using all range errors within ± 40 m of the mode of the error distribution. We refer to μ as the “bias” of the estimator, σ as the “fluctuation,” and F as the fraction of “outliers.” We consider a range estimate to be “reliable” when it has low bias and relatively few outliers. These statistics are presented in each panel of Fig. 7, where the Gaussian fit to the mode of the error distribution is also shown. Range errors are also summarized for a larger set of receiver depths in Table II for bias, Table III for fluctuation, and Table IV for percentage of outliers.

There are some depths where M0 delivers range estimates with relatively low bias (e.g., 330, 2976, 3521 m) or

few outliers (e.g., 330, 3521, 4012 m). At most depths, however, this method does not perform well in one or both categories, such that the median bias over depths is 186 m and the median number of outliers in error by more than 200 m is 55% (Table V).

There are two principal reasons for the problems suffered by M0. (1) Discrepancies between the relative amplitudes in the synthetics and observations can cause a misalignment of the synthetic and observed records upon cross correlation. An example of such an amplitude discrepancy is presented in Fig. 5 for a depth of 330 m. This can lead to bi- or multi-modal error distributions, and is probably best exemplified by the error distribution at 530 m depth in Fig. 7. At this depth, the cross correlations are commonly multi-peaked due to different alignments between the largest

TABLE II. Summary of performance of the four ranging methods—bias (m).^a

Depth (m)	M0	M1	M2	M3
210	-297.0	1.8	3.2	-297.0
330	17.0	19.4	15.2	17.0
530	152.3	39.9	14.5	20.2
751	219.5	31.3	19.8	18.3
1012	225.5	280.9	10.6	0.1
1332	224.4	19.2	7.4	4.8
1532	264.5	263.6	252.7	7.3
1992	412.5	16.5	13.0	0.7
2493	16.0	18.4	0.6	-1.6
2976	46.7	4.8	-3.1	-4.4
3521	-6.8	-16.3	-15.8	-6.8
4012	-34.6	-32.4	-24.6	-34.6

^aThe mean of the Gaussian function fit to the largest amplitude lobe of the error distribution, rounded to the nearest tenth of a meter.

TABLE III. Summary of performance of the four ranging methods—fluctuation (m).^a

Depth (m)	M0	M1	M2	M3
210	9.9	23.6	11.6	9.9
330	14.9	19.2	14.8	14.9
530	20.9	22.2	17.2	14.7
751	27.2	22.4	12.5	13.5
1012	21.8	18.6	13.5	10.2
1332	23.2	17.7	13.1	8.8
1532	23.9	18.9	13.8	11.0
1992	23.7	15.2	11.3	8.9
2493	19.5	19.3	10.3	8.8
2976	17.1	17.5	10.8	9.9
3521	9.7	18.7	9.5	9.7
4012	16.9	21.8	20.2	16.9

^aThe standard deviation of the Gaussian function fit to the largest amplitude lobe of the error distribution, rounded to the nearest tenth of a meter.

TABLE IV. Summary of performance of the four ranging methods—outliers.^a

Depth (m)	M0	M1	M2	M3
210	53.9%	3.4%	6.2%	53.9%
330	18.9%	1.6%	0.6%	18.9%
530	38.9%	1.7%	3.5%	0.6%
751	62.9%	1.9%	0.6%	0.0%
1012	83.9%	48.2%	15.1%	1.3%
1332	70.0%	30.1%	9.7%	0.1%
1532	90.7%	72.1%	82.2%	0.0%
1992	56.9%	54.4%	20.4%	0.0%
2493	57.0%	3.5%	9.3%	0.1%
2976	44.2%	1.9%	1.3%	1.1%
3521	3.4%	0.3%	0.2%	3.4%
4012	1.5%	0.0%	25.5%	1.5%

^aThe fraction of the range estimates with an absolute error greater than 200 m, rounded to the nearest tenth of a percent.

amplitudes in the synthetic and observed records as the relative amplitude content of the observations changes with time. Typically, different peaks of the error distribution occur during discrete time intervals, rather than moving continuously in a gradually changing fashion. This explains the discrete jumps of the range estimate between narrow, separated peaks in the error distribution, as opposed to a more continuous evolution. (2) Errors in the travel times of the peaks in the synthetics can bias range estimates, particularly when the finale is poorly predicted by the synthetics and has the largest amplitudes. This is true in the deep sound channel, and it is the reason for the large range biases seen between depths of 500 and 2000 m (Table II). At this depth, the ranging method shifts the latest arrivals in the synthetics to match the latest arrivals in the data, and the systematic mis-prediction of the latest travel times causes the estimator to be biased.

C. Refined ranging methods—Methods 1, 2, and 3

M0, the direct cross correlation of the observed and synthetic records, is not a reliable range estimator in that it commonly produces significant bias and a large number of outliers. It overemphasizes large amplitude peaks and late arrivals that the synthetics have difficulty fitting. The problems encountered with M0 can be ameliorated by down-weighting the amplitudes or eliminating late arriving peaks in some way prior to or during the comparison between synthetic and observed waveforms. The three refined methods

aim to improve ranging performance in different ways, but are straightforward to implement in practice. Compared with M0, we seek methods that are less biased, generate fewer outliers, and have lower sensitivity to the parts of the data records that are poorly fit by the synthetics (and therefore the aspects of the ocean model that are most erroneous).

1. Method 1 (M1)—The telegraphic signal

M1 reduces the influence of the high amplitude arrivals by converting both synthetic and observed waveforms into “telegraphic signals” prior to cross correlation. However, it retains the finale in the comparison between the observed and synthetic telegraphic waveforms. The telegraphic signal is a binary signal composed of a series of 1 s and 0 s such that 1 s are assigned to the parts of the signal above a threshold amplitude and 0 s are assigned otherwise, as Figs. 8(a) and 8(b) illustrate. We refer to each continuous series of 1 s in the waveform as a “panel,” and the set of panels that define a waveform as the “panel structure.” The threshold level is a variable of the method, but we set it to three times the rms value of trailing noise in the observed waveform. To apply the threshold to the synthetic waveform, we compute the ratio of the peak amplitude to the threshold level of the

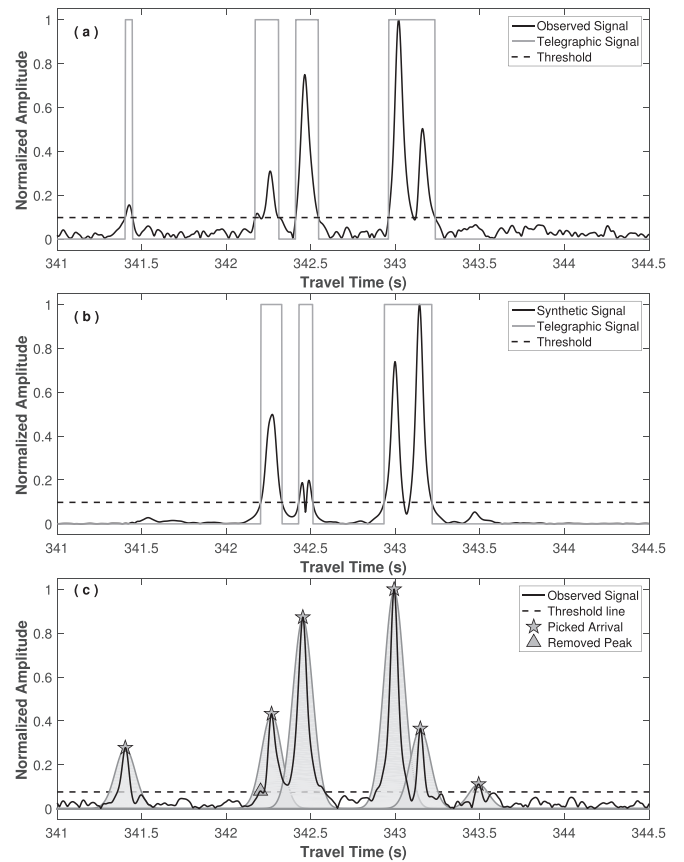


FIG. 8. (a), (b) Illustration of the generation of the telegraphic signal in M1 from (a) an observed data record from a single ping and (b) a synthetic record. The dashed line specifies the threshold level used to define the panels that compose the telegraphic signal. The depth of the receiver here is 330 m. (c) Illustration of travel time picks for M2. The local maximum is measured directly for all peaks above a threshold (dashed line), and small side peaks are removed within the “shadow” of a larger peak, which is defined in Sec. IVC2.

TABLE V. Summary of range errors over receiver depth.

Method	Median bias (m) ^a	Median % outliers ^b
Direct correlation, M0	186	55.4
Telegraphic signal, M1	19	12.7
Travel time, M2	14	7.8
Eliminate finale, M3	7	0.9

^aThe median of range bias (m) over the 12 receiver depths in Table I.

^bThe median of percent range errors > 200 m over the 12 receiver depths in Table IV.

observed record and then choose the threshold level for the synthetic that gives this same ratio relative to its peak amplitude. The telegraphic signal effectively gives the same weight to all arrivals in the computation of the cross correlation, irrespective of the amplitude of the peak as long as the peak is above the threshold level. In effect, this down-weights differences in amplitudes between the synthetic and observed waveforms and de-emphasizes the largest amplitude peaks, which at some depths are in the parts of the observed record most poorly fit by synthetics. In particular, it down-weights the influence of the finale at depths where it has especially large amplitudes (e.g., in the deep sound channel).

Figure 9 presents distributions of ranging results for M1 at six receiver depths. Bias is reduced substantially relative to M0, although outliers still exist at some depths and multimodality has not been eliminated entirely. The median bias over range is 19 m, and the median number of outliers in error by more than 200 m is about 13% (Table V). Based on these statistics, we conclude that M1 is generally a reliable estimator, particularly in comparison to M0. However, the principal drawback of M1 is that there continues to be a substantial number of outliers for receivers in the deep sound channel, notably from about 1000 to 2000 m. In addition, although bias has been greatly reduced compared to M0, it remains non-negligible and, as discussed later, is significantly above the level caused by travel time variations expected by changes in ocean state.

2. Method 2 (M2)—Travel time measurement

Another way to reduce the effect of large amplitude arrivals is to ignore amplitudes entirely, and use travel time observations as the basis for ranging. We measure or “pick” arrival times of synthetics and observations for peaks above the same threshold level used in M1, but de-emphasize small

amplitude side peaks near larger peaks. Figure 8(c) presents an example of travel times picked on one record. Figure 8(c) illustrates how small amplitude side peaks are identified in the “shadow” of larger nearby peaks on one record. The shadow area of a peak is defined as the area within a Gaussian function whose amplitude and time center are the same as the peak, but the width is increased. Here, the width of the shadow is defined as 72 ms, which is about triple the width of peaks in the observed records. We consider the smaller amplitude side peaks, which actually occur quite often, to be noise, and eliminating them improves this method. Another approach would be to treat the side peaks as scattering from small-scale heterogeneities (e.g., Dzieciuch, 2014), but this is outside the scope of this paper.

We minimize the difference between the travel time observations (t_m^o , $1 \leq m \leq N_o$) and synthetic travel times (t_n^s , $1 \leq n \leq N_s$) by performing a time shift, δt , of the synthetic relative to the observed waveform. One complication is that the numbers of observed (N_o) and synthetic (N_s) travel times often differ from one another. One method that works reasonably well to estimate δt is to maximize the following functional:

$$G(\delta t) = \sum_{m,n} \exp \left[\frac{-(t_m^o - t_n^s - \delta t)^2}{2\sigma^2} \right], \quad (7)$$

where we set $\sigma = 24$ ms, which is about the width of the peaks in observed and synthetic signals. The results are presented in Fig. 10.

For M2, the median bias over the range is 14 m, and the median number of outliers in error by more than 200 m is about 8% (Table V). Based on these statistics, we conclude that M2 is generally a reliable estimator, particularly in comparison to M0, and M2 also performs better than M1 in both

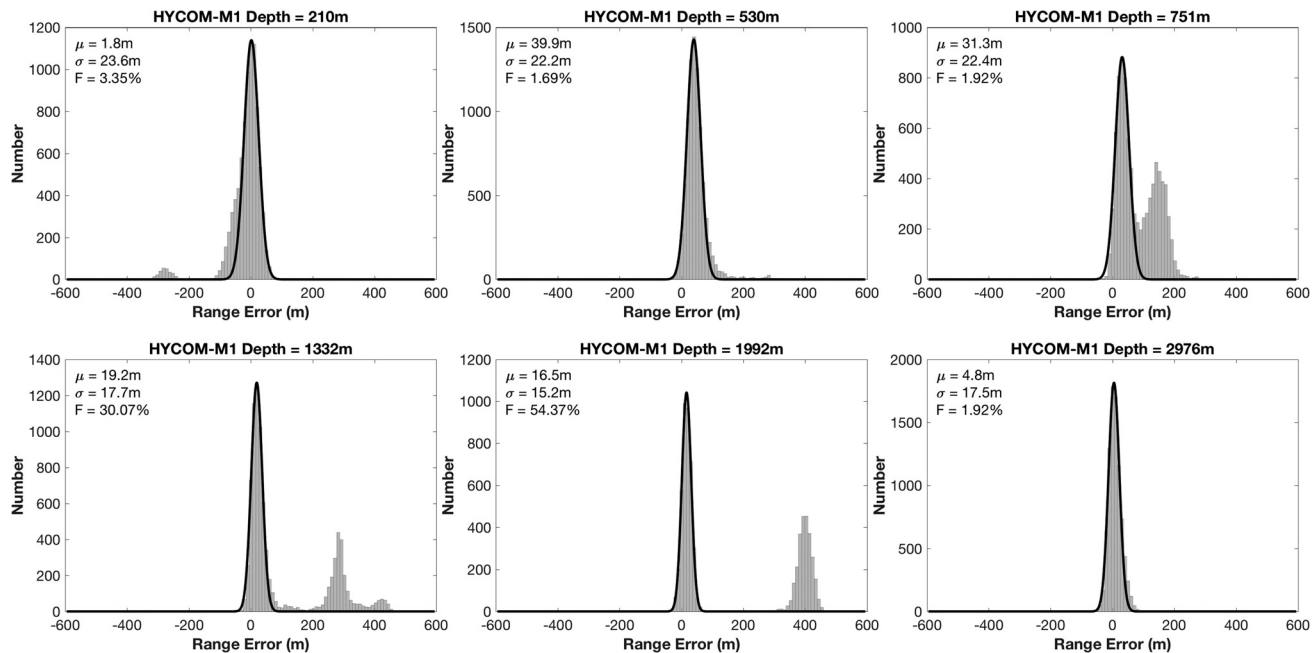


FIG. 9. Similar to Fig. 7 but for ranging method 1 (M1).

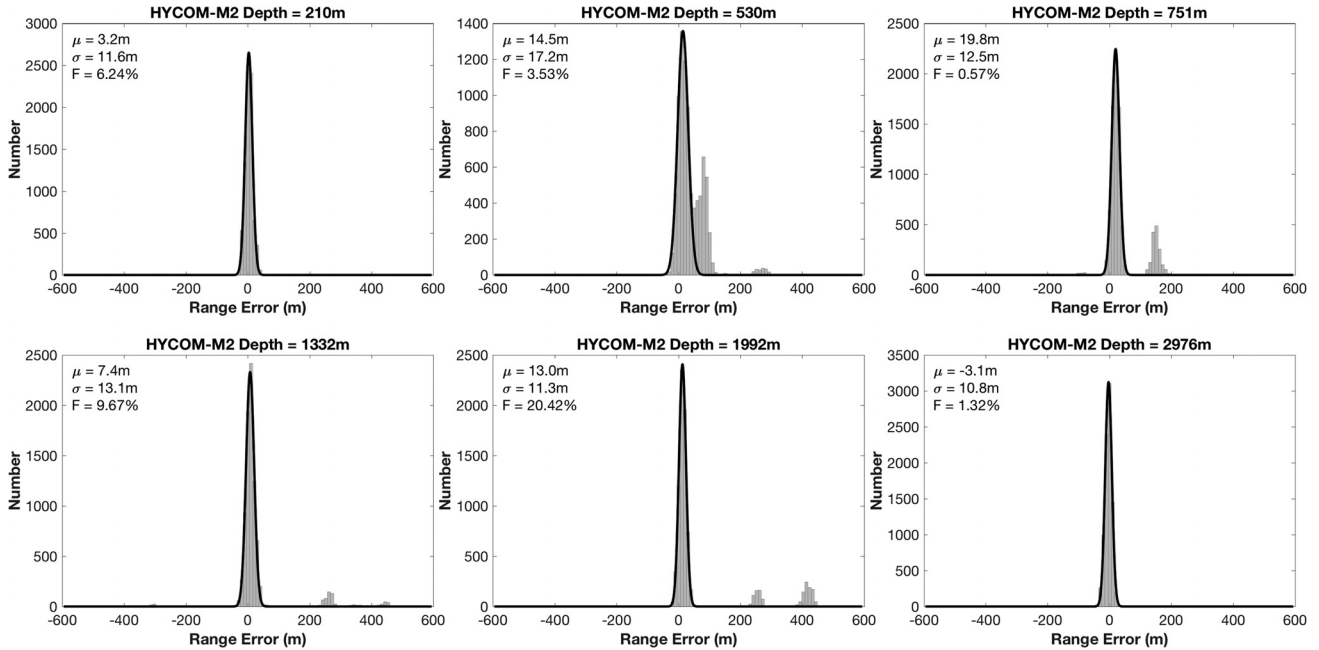


FIG. 10. Similar to Fig. 7 but for ranging method 2 (M2).

bias and outlier generation. However, although we do not show this here, the performance of M2 is strongly dependent on the ocean model used, and the sensitivity of the results to the ocean model may be a principal drawback of this method.

3. Method 3 (M3)—Reject the finale

Ranging method 3 compares synthetic and observed waveforms by direct cross correlation, like M0, but eliminates the finale of both observed and synthetic records from the comparison. The “finale” can be defined in many ways. We define it as those parts of the observed or synthetic waveforms that arrive after the dashed black line in Fig. 4(b). That line is chosen because after it peak times in the data and synthetics begin to differ from one another appreciably. The finale of the waveform comprises ray identification numbers ≤ -21 or $\geq +22$, which correspond to rays with upper turning points deeper than about 400 m and lower turning points shallower than about 3100 m. With this definition, rays with small and median launch angles shown in Fig. 11(a) would be in the finale but the rays with a large launch angle would not. From a normal mode perspective, the finale is composed almost exclusively of modes numbered between 1 and 100, as Fig. 11(b) illustrates.

Effectively, therefore, we aim to eliminate rays that turn in the mid-ocean. Rays with shallower upper turning points and deeper lower turning points sample a substantial fraction of the ocean column so that depth-limited errors in ocean models will have a weaker effect on the range estimates. In addition, ocean models may be more accurate at shallower depths, where satellite data provide direct constraints. Synthetics diverge from observed waveforms for the later arrivals because the deep sound speed channel in the ocean model is constrained more weakly by surface observations and may be influenced more by internal wave fluctuations. For this reason, in M3 we seek to focus comparison between

observations and synthetics on the arrivals that sample most of the ocean column, if possible. To affect this constraint, before cross correlation we set the synthetic and observed waveforms to 0 after the onset time of the finale, identified by the black dashed line in Fig. 4(b). We believe any ranging method can be improved, on average, by removing the finale.

Because the finale has been entirely removed from consideration, ranging results that emerge from M3 (Fig. 12, Tables II–IV) are better than those from M1 and M2. The median bias over the range is 7 m and the median number of outliers in error by more than 200 m is about 1% (Table V). This is particularly true for receivers near the middle of the deep sound channel (e.g., ~ 1500 m), which are strongly affected by channel-propagating waves, and where substantial outliers resulted from M1 and M2. The principal exception is for the shallowest and deepest receivers, where the method actually reverts to M0 because there is no finale at those depths. This depth range defines the principal drawback for M3 and suggests that at these depths another method may be preferable.

D. Sensitivity to the starting range estimate R_0

The ranging methods considered here are all based on measuring the shift in range, δR , from an initial range estimate, R_0 , which is the range at which the synthetics are computed. The statistics presented in Tables II–V arise when the initial range estimate is approximately equal to the ground truth range, i.e., $R_0 \approx R_{GT}$. We now ask: what will happen to these statistics when R_0 differs from R_{GT} ?

To first order, we expect that a relatively small change in range will principally shift and not deform the synthetics. Therefore, we expect only weak sensitivity of range estimates (R) to variations in the range at which the synthetics are computed (R_0). As Fig. 13 shows, however, the synthetics do not just shift in time when the range is changed, they also stretch

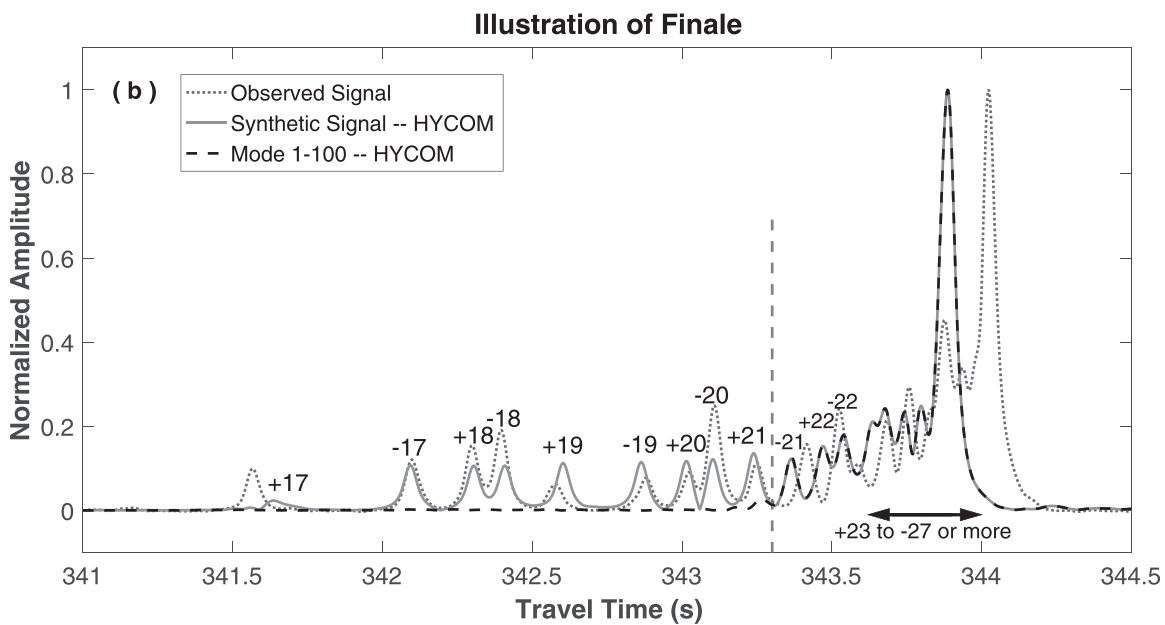
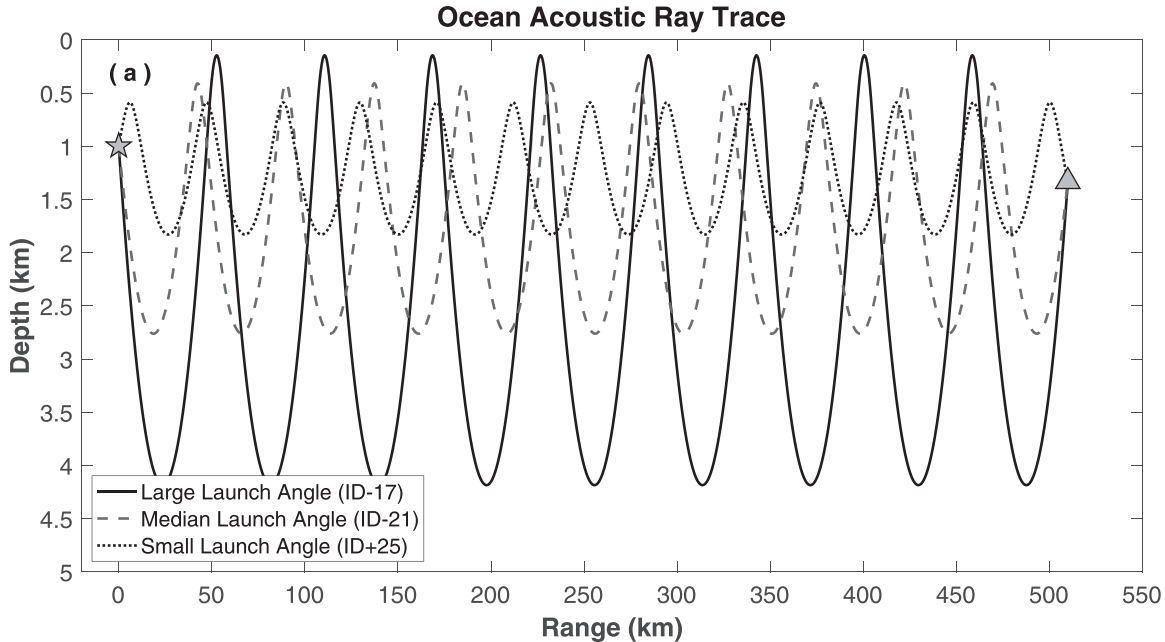


FIG. 11. Eliminating the finale in M3. (a) Paths for three rays terminating at a receiver at a depth of 1332 m. Steeply launched rays sample much of the water column, whereas rays launched at less steep angles compress into the deep sound channel. (b) Illustration of the finale being composed of modes 1–100. The grey line is the observed record, the black line is the complete synthetic, including all modes 1–250, and the dotted line is the synthetic including only modes 1–100. The vertical dashed line indicates the time of onset of the finale, defined in Fig. 4(b). Ray IDs of some peaks are indicated.

or compress in time and there are other changes such as the number of resolved peaks. Thus, there are actually subtle but important changes in the synthetics, both in relative arrival times and amplitudes, when R_0 changes. It is, therefore, important to determine how the range error statistics we present depend on the initial range used to compute the synthetics.

Figure 14 shows how statistical estimates of bias, fluctuation, and percentage of outliers (in error by more than 200 m) vary as a function of the deviation of R_0 from R_{GT} (i.e., $R_{GT} - R_0$) for three depths: 530 m, 1332 m, and 2976 m. The results presented in Tables II–V appear when the horizontal axis on each plot is equal to 0. The conclusion is that the optimal values of bias, fluctuation, and outlier production do not generally occur when $R_0 = R_{GT}$ and change slowly as

R_0 diverges from R_{GT} . The statistics presented in Tables II–V here change only in detail when the initial range is changed by up to ± 2 km from the ground truth range. Thus, the principal conclusions of this study are robust relative to changes in the initial range up to at least 2 km. Moreover, this conclusion is extendable to much larger errors in the initial range estimate (~ 10 km) if the range methods are iterated, which we do not do here, however.

V. DISCUSSION

A. Overview

Ideally, a ranging algorithm would produce range errors with a probability distribution that is predominantly uni-modal

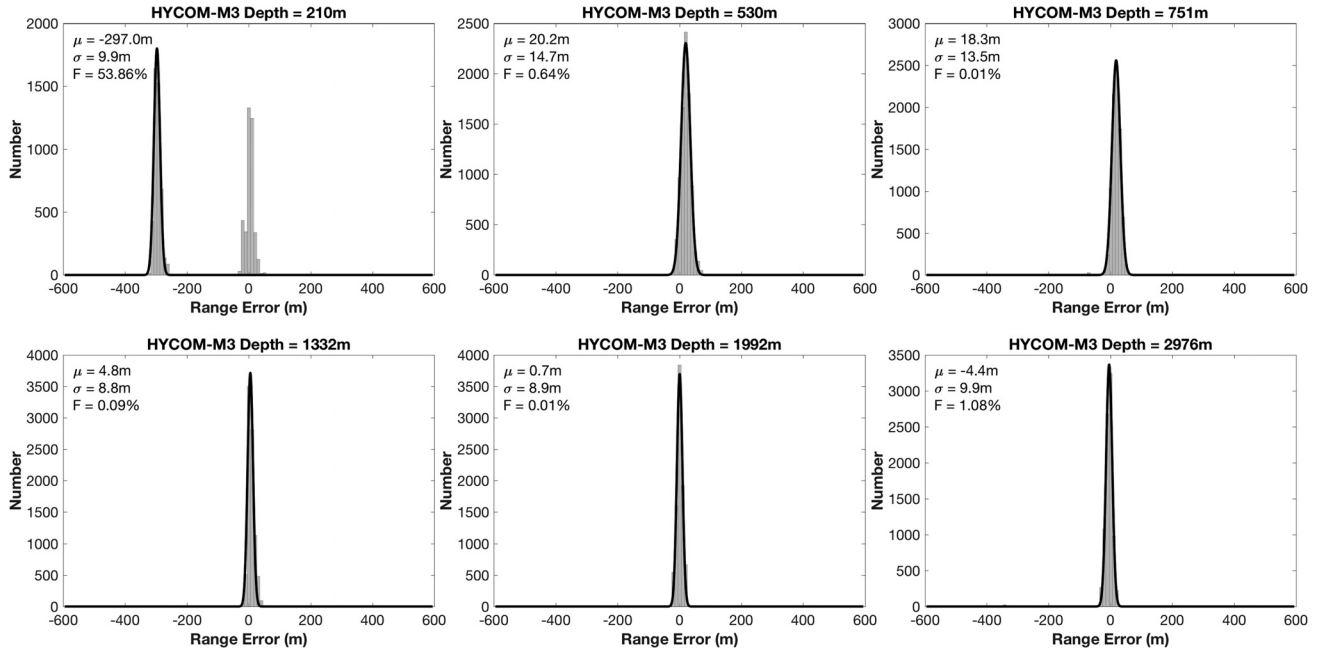


FIG. 12. Similar to Fig. 7 but for ranging method 3 (M3).

so that outliers are rare, possess small systematic errors or bias, and have a small standard deviation or fluctuation. Of these characteristics, the first two, small bias with few outliers, are particularly important. For range estimates, fluctuations within a uni-modal distribution are inevitable due to variations in ocean state, and minimizing fluctuations requires precise knowledge of variations in ocean structure. Our principal conclusion is that each of the ideas represented by methods 1–3 (amplitude normalization, travel time measurements, rejection of the finale) substantially improves the range estimator by reducing the incidence of outliers, reducing bias, and making the method less sensitive to differences between the ocean models. It remains to discuss here stationary and time-variable range errors that characterize the refined ranging methods.

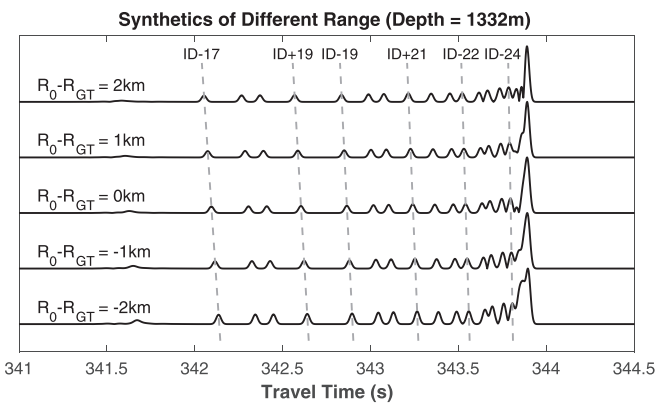


FIG. 13. Plots of synthetics through the HYCOM model for a receiver at 1332 m depth (transmitted at 998 m depth) for different ranges, where $R_{GT} \sim 510$ km. Traces are aligned to the one where $R_0 - R_{GT} = 0$, shifting by a time equal to $R_0 - R_{GT}/1480$, which approximately aligns the largest amplitude peak in the finale. These results illustrate that changing the range up to ± 2 km not only shifts the waveforms, but also stretches them (as evidenced by the slopes on the dashed lines) and changes their relative amplitudes. Ray IDs of some peaks are indicated.

B. Range errors not caused by changes in ocean state

What are the causes of systematic error or bias in range estimates that are observed using M1 to M3? First, static errors in the ocean model produce a range bias of more than 100 m at many receiver depths for M0. M1 to M3 are designed to reduce the effect of such errors in the ocean model, and the reduction in bias evidenced by M1 to M3 compared to M0 is an indication that they have been quite successful. Second, independent of errors in the ocean model there are other sources of experimental error, including uncertainty in the transmitter's location (<5 m), uncertainty in each receiver's location (5 m) and depth (2 m), errors caused by the use of a range-independent ocean model (5 m), and approximations in the synthetics such as the flattening transformation (<1 m) and the computation of distances along a great-circle on the oblate spheroid (<1 m). Some of these effects may offset one another, and together they contribute an experimental error of about 10 m, which may be time invariant and would define a bias floor for any method used to estimate absolute range.

Therefore, range bias largely results from the residual effects of static errors in the ocean model, as well as other sources of uncertainty, particularly in the experimental setup. The 7 m median bias found for M3 is about as low as could be expected for any absolute ranging method, given the level of experimental error in this study. Larger biases observed for M1 and M2 above the level of experimental error probably result from greater sensitivity to errors in the ocean model than M3.

C. Range errors caused by changes in ocean state

Fluctuations in range errors are largely (but not exclusively) attributable to time variations in ocean state. Time variations in ocean state have two principal effects on the

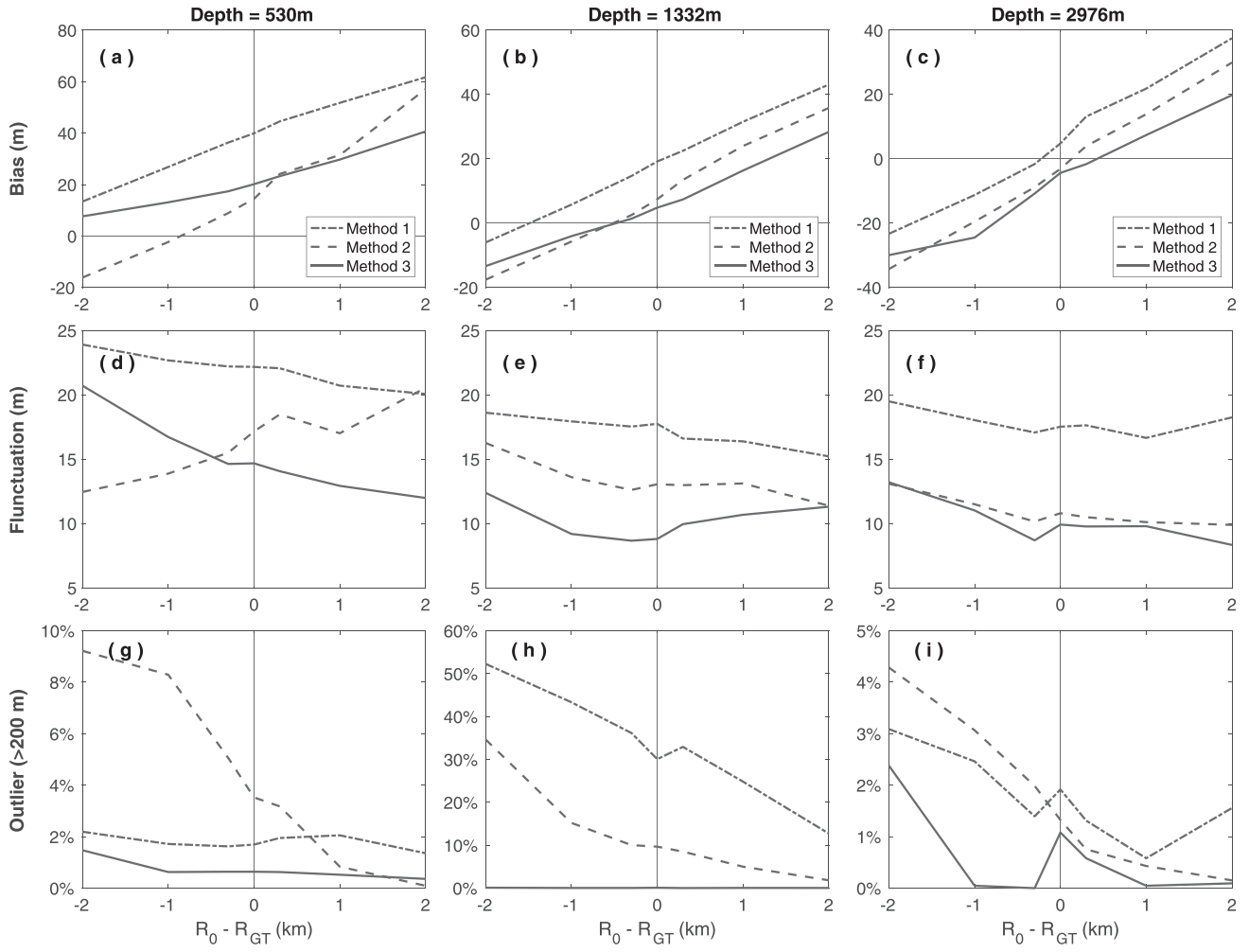


FIG. 14. The effect on the range statistics of changing the initial range, R_0 , used to construct the synthetics in the ranging methods where results are shown for receiver depths of (left column) 530 m, (middle column) 1332 m, and (right column) 2976 m. Rows are different statistics: (top row) bias μ , (middle row) fluctuation (σ), and (bottom row) percent outliers with range errors greater than 200 m (F). Results are presented as functions of the deviation of the initial range from the ground truth range, R_{GT} . The y axis ranges for different depths are different.

waveforms: (1) they produce variations in the time of arrival of the peaks in the acoustic waveforms, and (2) they have an even larger effect on the relative amplitudes of the peaks. Figure 15(a) illustrates the variations of the travel times of the 18 peaks that constitute the observed waveforms at a depth of 1332 m. The ray IDs of some of the peaks are shown in Fig. 15. These arrival times have been corrected for receiver drift, effectively correcting to a common transmitter-receiver range. Figure 15(b) presents the standard deviation of the amplitude and reduced travel time of each of the 18 peaks seen at 1332 m depth. Both travel time and amplitude variations grow later in the record, particularly in the finale. Ray IDs link Fig. 15 to Figs. 4, 11, and 13.

Figure 16(a) tracks the observed change in arrival times in detail over the three days of the experiment for the receiver at 1332 m depth. These arrival times are determined from those shown in Fig. 15(a). At this depth we see 18 peaks, but the times presented in Fig. 16(a) are the average time shift only of peaks 2–14, which corresponds to ray IDs –17 to –23, where the mean arrival time of each peak has been removed. We have not included the first peak because it is not well represented in the synthetics or the last four peaks because they are difficult to resolve unambiguously.

A clear semi-diurnal pattern (12-h period) in the arrival times is observed with a larger amplitude earlier in the record, presumably caused by temperature variations associated with internal tides (e.g., Dushaw *et al.*, 1995; Dushaw and Worcester, 1998; Dushaw *et al.*, 2011). There is also a secular variation, a steady downward trend during the three days of observation. Finally, there are higher frequency variations perhaps caused by internal waves. The rms variation of the arrival times is 6.4 ms with a peak-to-peak span of about ± 20 ms. We convert the observed time shifts to shifts in the range, which we present as the black lines in Figs. 16(b)–16(d). The rms variation in arrival times converts to an rms range shift of about 9.5 m, and the peak-to-peak span is an apparent range variation of about ± 30 m. We attribute these changes to changes in ocean state.

For M1 and M2, the fluctuations in the range estimates listed in Table III are typically larger than the 10 m expected to be caused by changes in ocean state alone. This means that for these methods, the range fluctuations are caused only in part by changes in ocean state, and other physical processes must also contribute. Fluctuations for M3 tend to be closer to the 10 m expected for changes in ocean state alone. From this we hypothesize that the fluctuations in range

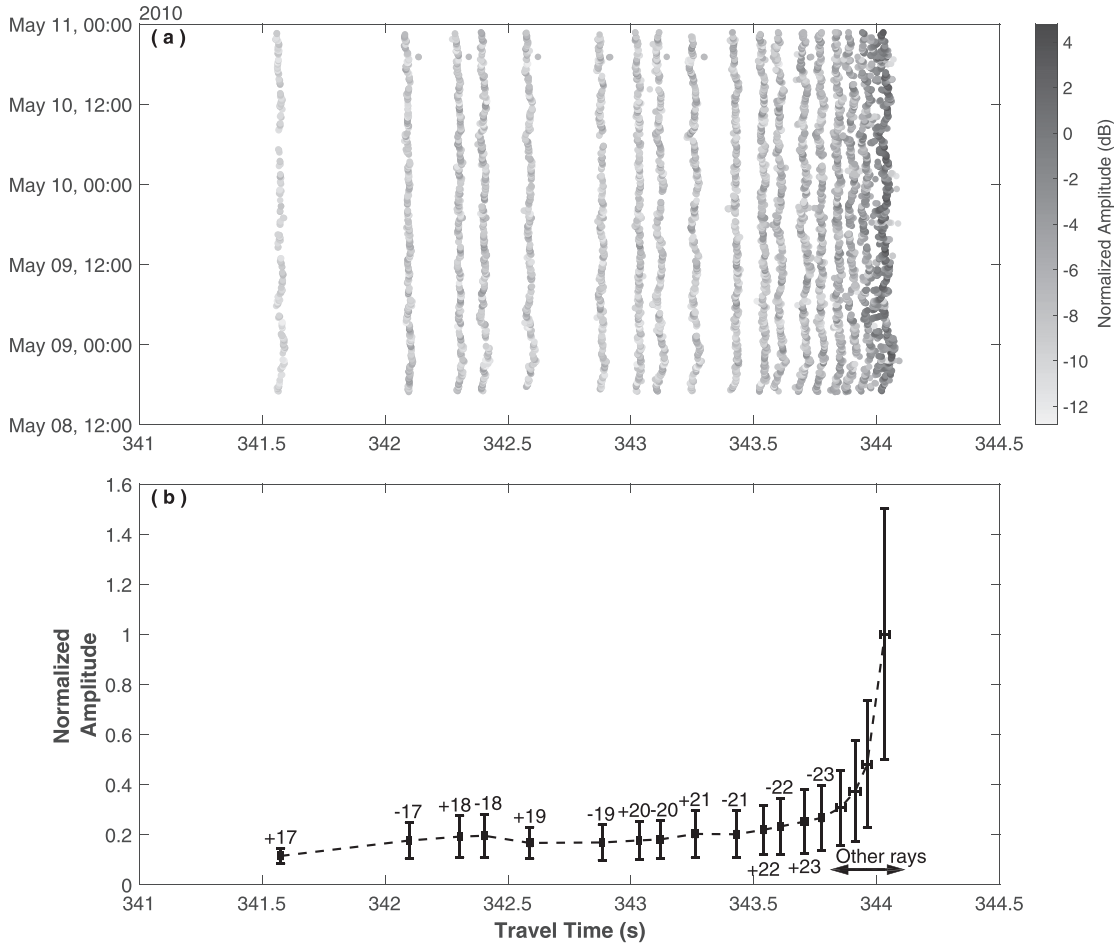


FIG. 15. Variation in travel times and amplitudes for observed peaks at a receiver depth of 1332 m. (a) Each dot is from a stack of six pings, plotted at the reduced travel time of each peak, which has been corrected for time variations of the receiver location. Amplitudes are shaded grey. (b) Summary of the variations (standard deviation) of travel time and amplitude over the entire experiment from the data shown in (a). Reduced travel time variations are believed to be caused mostly by changes in ocean state. Ray IDs of some peaks are indicated.

estimated by M3 are almost exclusively produced by ocean state changes. In other words, M3 appears to be able to track changes in ocean state with high fidelity.

To check this, Figs. 16(b) compares how the range estimates from M3 track the observed variations in travel time. There is an offset (bias) of about 7.7 m between the black (observation) and grey lines (results of ranging), reflecting the bias we attribute to experimental errors. However, the range estimates clearly track at least the semi-diurnal part of the travel time variation. The standard deviation of the range estimates is about 10.5 m, close to the 8.9 m of the observed travel time variations. The rms of the residual between average-removed observed and estimated range variation decreases to 7.1 m, which illustrates the good correlation between M3 range estimates and observed travel time variations. Therefore, at least for M3, the observed fluctuations in range result in large part from fluctuations in travel time caused by changes in ocean state (dominantly tidal effects).

M2 [Fig. 16(d)] tracks the semi-diurnal variation in travel times less faithfully, but still well. The standard deviation is about 13.3 m, although the bias (~ 8.7 m) is similar. And the residual rms is 10.4 m, also illustrating that M2 tracks observations worse than M3. In contrast, the range

estimates from M1 track the travel time variations much worse than the other ranging methods [Fig. 16(c)]. Both average and fluctuations are much higher: 22.0 m and 15.4 m, respectively. The reason for this in M1 (and to a lesser extent M2) is the residual effect of the finale. Time variations in ocean state do not just change travel times, they also change the amplitude structure of the waveforms, particularly in the finale as Fig. 6(c) illustrates. This affects the panel structure of the telegraphic signals, which impacts the range estimates. The effect is weaker on the travel time measurements that compose M2 than on the telegraphic signals, which compose M1. This is the reason why M1 shows a larger fluctuation, on average, than either M2 or M3. Therefore, we believe that fluctuations above the 10 m level are also caused by time variations in ocean state, but by effects on amplitudes rather than on travel times.

D. Relative merits and joint use of M1 to M3

M3 appears to be the most successful of the ranging methods presented: it has the lowest bias, the fewest outliers, and tracks travel times most faithfully of the three refined methods. M1 and M2 are essentially equally reliable for the data set and ocean model used here.

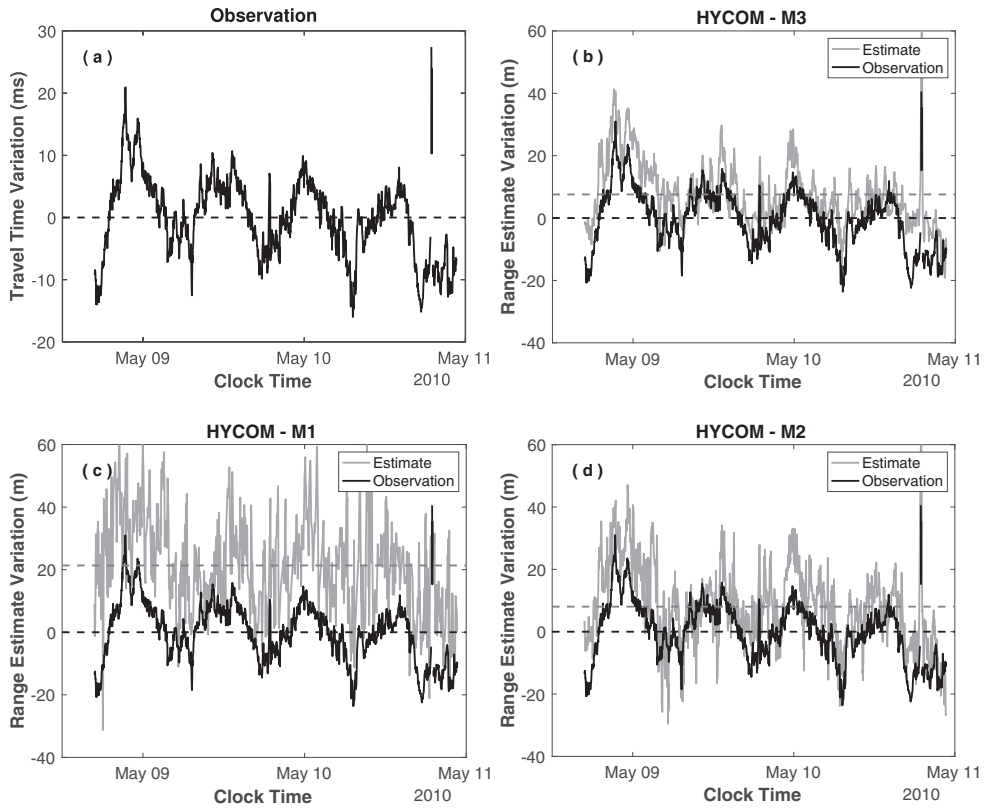


FIG. 16. (a) Variations in observed travel times corrected for variation in receiver location at 1332 m depth. Travel time variations for each of peaks 2–14 (prior to the finale) are measured relative to the mean of each peak and averaged. Each measurement is an average over six pings, and the data are the same as in Fig. 15(a). A strong semi-diurnal signal is observed, which we attribute to tidal effects on ocean state. (b) Observed travel time variations are converted to range variations by multiplying by 1480 m/s (black line) and compared to the variations in range estimates relative to ground truth from M3 (grey line). M3 tracks the apparent range shifts caused by tidal effects quite well. The grey dashed line is the mean of the range estimates; its deviation from the black dashed line indicates the bias of the method. (c) Same as (b), but the grey line is from M1. (d) Same as (b), but the grey line is from M2. The larger fluctuation in range estimates, particularly using M1, obscures the semi-diurnal tidal signal more than from M3.

Although the ideas that define M1 to M3 are applied separately, they could be applied in tandem and further refinement, perhaps location specific, could be introduced to improve the techniques. For example, M3 does not outperform M1 at depths less than 500 m or deeper than 3500 m, so it may be advisable to use the two methods together and give different weights to them based on water depth. In addition, ranging methods deployed in the field can bring in other information to guide the range estimates, which we do not invoke here. For example, the past history of range estimates can be used to determine if a new range estimate is worth retaining. In contrast, in our tests we consider each ping to present an independent measurement. Multiple transmitters also could be used to provide more quality control. It may also be advisable to use more than one ocean model in ranging in addition to applying more than one ranging method. Finally, relative location information could be incorporated to provide the distance to the previous range estimate by, for example, cross correlating signals from different pings.

VI. CONCLUSIONS

Two principal questions motivate this study. First, what are the general characteristics of absolute ranging methods that can be used to extract reliable range estimates based on an ocean general circulation model? Second, how well will

such an ocean model perform as the basis for long-distance acoustic ranging between an acoustic transmitter and a submerged receiver in a deep water setting?

To address these questions we employ acoustic data from the PhilSea10 experiment, which have the beneficial characteristic that transmitter and receiver locations are relatively fixed and known during the more than 50 h of acoustic transmission and data recording. Thus, we have a good estimate of the ground truth range for each ping. As the ocean model we use a path-averaged (range-independent) and time-averaged (three-day average around the time of the experiment) HYCOM model. The synthetic method is an adiabatic normal mode method of our own construction.

The simplest ranging method that we considered (method 0), direct cross correlation between observed and synthetic waveforms to estimate a time shift between the records, does not perform well based on the HYCOM model. The bias of the estimator and outlier generation were too strong for this method to be considered reliable. This method does not work well at most depths due to its attempt to align the largest amplitude peaks in the data and synthetics, which may be for different arrivals in the two records or in the finale of the record, which is poorly predicted by the synthetics.

In contrast, the refined ranging methods (M1 to M3) performed reliably based on the HYCOM model. The key feature of the refined ranging methods is that they weigh down

those aspects of the data that are most different from the synthetics. M1 to M3 de-emphasize in different ways the largest amplitude peaks and/or the latest arrivals (the finale) either by normalizing amplitudes (M1), using measured travel times (M2), or rejecting the parts of the waveforms later than a critical time (M3) in order to de-emphasize the effect of the finale. We present M1 to M3 as an answer to the first question that motivates this study.

What is meant by reliable in the assessment of the models and the ranging methods will be application specific. But, for our purposes we consider a reliable estimator to produce range errors characterized by a bias of ~ 20 m or better, a Gaussian fluctuation of ~ 20 m or better, with less than $\sim 10\%$ of estimates in error by more than 200 m. These characteristics are common for M1 to M3, although at some depths and for some methods the results may be considerably better than this. Therefore, these statistics provide the answer to the second question that motivates this study.

This study shows that it is possible to obtain accurate real-time range estimates between submerged objects based on a general ocean circulation model, and the HYCOM model accurately predicts at least the earlier arrivals. In the future, with enough transmitters or receivers, the range to and movement of undersea objects can be obtained at considerable distances in deep water. With well-designed distributions of receivers and transmitters, such estimates may prove useful to calibrate ocean circulation models.

Further reduction in the bias of the range estimator may require ocean models that can reliably predict travel times at a distance of 500 km better than 15 ms (or four parts in 10^5). Reducing fluctuations will require predicting or reducing sensitivity to semi-diurnal tide-induced fluctuations in ocean state (likely including the semi-diurnal internal wave spectral peak, in addition to direct effects of tidal flows), which we observe is the principal component of the travel time fluctuations. Finally, to reduce outliers may require more sophisticated ranging methods than we have deployed, which are not as easily confused by time-variable differences between observed and synthetic waveforms. Incorporating relative location information by, for example, cross-correlating signals from different pings may prove to be particularly advantageous in this regard.

It is important to acknowledge that the range error statistics presented here derive from a very specific experimental setting: there is only one location (the Philippine Sea), one range (~ 510 km), one transmitter depth (~ 998 m), one frequency band (centered near 200 Hz), the results are only over three days, one type of transmitted signal (an M-sequence), and the experiment is in very deep water. The principal variable is receiver depth. Some of these characteristics may represent a best case scenario for ranging. For example, the water in the central Philippine Sea is very deep so there is no need for the synthetics to model seafloor interaction through modal-coupling or some other method. In addition, the location is well separated from major current systems (e.g., the Kuroshio or Gulf Stream) that are particularly challenging for ocean models to reproduce accurately and in which there is likely to be greater spatio-temporal variability than in the region of study. Other characteristics of

the experimental configuration provide a greater challenge for ranging, however, such as the transmitter depth, which couples a great deal of energy into the deep sound channel. This produces a strong finale in the observed records, which is precisely the signal that the synthetics struggle to fit. On balance, however, experiments performed under very different (and less ideal) conditions than the one we consider may very well produce larger range errors.

Nevertheless, we believe that the general principles established about successful ranging methods paired with general circulation models will hold broadly and may prove to be widely transportable. These principles are the answer to the first question that motivates this study, which is summarized by the following two points: (1) It is useful to compare observed and synthetic waveforms to obtain absolute range estimates and use as much of the waveforms as possible. (2) However, ranging methods should be tuned to accentuate the parts of the data records most likely to be reproduced reliably by ocean models through the synthetics. Which parts of the data these are may vary from place to place, but they will generally depend predominantly on features of the synthetics that are most accurate and least sensitive to errors in the ocean model or differences between ocean models. As an example, we have found it useful to eliminate amplitudes from consideration as they are not well reproduced by synthetics and fluctuate strongly with ocean state. In addition, we have found it useful to focus on waves that sample the entire ocean rather than those that are trapped in a waveguide, as range estimates based on them are believed to be more robust to errors in the ocean model (and differences between ocean models).

ACKNOWLEDGMENTS

The authors thank five anonymous reviewers and the Associate Editor, Kainam Thomas Wong, for critical comments that helped to improve this paper. They also thank the developers of the Gibbs SeaWater (GSW) Oceanographic Toolbox of TEOS-10 and the HYCOM ocean model. Funding for the development of the HYCOM model has been provided by the National Ocean Partnership Program and the Office of Naval Research. Data assimilative products using the HYCOM model are funded by the U.S. Navy. Computer time was made available by the Department of Defense (DoD) High Performance Computing Modernization Program. The output is publicly available.¹ The Philippine Sea experiments and post-experiment data reduction were supported by the Long Range/Deep Water Propagation thrust area of the Ocean Acoustics Program at the Office of Naval Research under APL-UW Grant Nos. N00014-08-1-0843, N00014-08-1-0797, N00014-13-1-0009, N00014-15-1-2233, and N00014-18-1-2213, and Scripps Institution of Oceanography Grant No. N00014-08-1-0840.

¹See <http://hycom.org> (Last viewed November 27, 2019).

Andrew, R. K., Ganse, A., White, A. W., Mercer, J. A., Dzieciuch, M. A., Worcester, P. F., and Colosi, J. A. (2016). "Low-frequency pulse propagation over 510 km in the Philippine Sea: A comparison of observed and theoretical pulse spreading," *J. Acoust. Soc. Am.* **140**(1), 216–228.

- Andrew, R. K., Mercer, J. A., Bell, B. M., Ganse, A. A., Buck, L., Wen, T., and McGinnis, T. M. (2010). "PhilSea10 APL-UW cruise report: 5–29 May 2010," Technical Report APL-UW TR 1001 (Applied Physics Laboratory, University of Washington, Seattle, WA).
- Chandrasekhar, V., Seah, W. K., Choo, Y. S., and Ee, H. V. (2006). "Localization in underwater sensor networks: Survey and challenges," in *Proceedings of the 1st ACM international Workshop on Underwater Networks*, pp. 33–40.
- Chapman, C. (1973). "The Earth flattening transformation in body wave theory," *Geophys. J. Int.* **35**, 55–70.
- Chassignet, E. P., Hurlburt, H. E., Smedstad, O. M., Halliwell, G. R., Hogan, P. J., Wallcraft, A. J., Baraille, R., and Bleck, R. (2007). "The HYCOM (hybrid coordinate ocean model) data assimilative system," *J. Mar. Syst.* **65**(1), 60–83.
- Colosi, J. A., and Morozov, A. K. (2009). "Statistics of normal mode amplitudes in an ocean with random sound-speed perturbations: Cross-mode coherence and mean intensity," *J. Acoust. Soc. Am.* **126**(3), 1026–1035.
- Colosi, J. A., Scheer, E. K., Flatté, S. M., Cornuelle, B. D., Dzieciuch, M. A., Munk, W. H., Worcester, P. F., Howe, B. M., Mercer, J. A., Spindel, R. C., and Baggeroer, A. B. (1999). "Comparisons of measured and predicted acoustic fluctuations for a 3250-km propagation experiment in the eastern North Pacific Ocean," *J. Acoust. Soc. Am.* **105**(6), 3202–3218.
- Dosso, S. E. (2003). "Environmental uncertainty in ocean acoustic source localization," *Inverse Probl.* **19**(2), 419–431.
- Duda, T., Morozov, A. K., Howe, B. M., Brown, M. G., Speer, K., Lazarevich, P., Worcester, P. F., and Cornuelle, B. D. (2006). "Evaluation of a long-range acoustic navigation/thermometry system," in *IEEE Oceans Conference*, 18–21 September 2006, Boston, MA.
- Dushaw, B. D., Dzieciuch, M. A., and Worcester, P. F. (2009). "On the time-mean state of ocean models and the properties of long-range acoustics," *J. Acoust. Soc. Am.* **125**(4), 2492.
- Dushaw, B. D., Howe, B. M., Cornuelle, B. D., Worcester, P. F., and Luther, D. S. (1995). "Barotropic and baroclinic tides in the central north pacific ocean determined from long-range reciprocal acoustic transmissions," *J. Phys. Oceanogr.* **25**(4), 631–647.
- Dushaw, B. D., and Worcester, P. F. (1998). "Resonant diurnal internal tides in the North Atlantic," *Geophys. Res. Lett.* **25**(12), 2189–2192, <https://doi.org/10.1029/98GL01583>.
- Dushaw, B. D., Worcester, P. F., and Dzieciuch, M. A. (2011). "On the predictability of mode-1 internal tides," *Deep Sea Res., Part I* **58**(6), 677–698.
- Dzieciuch, M. A. (2014). "Signal processing and tracking of arrivals in ocean acoustic tomography," *J. Acoust. Soc. Am.* **136**(5), 2512–2522.
- Flatté, S. M., and Vera, M. D. (2003). "Comparison between ocean-acoustic fluctuations in parabolic-equation simulations and estimates from integral approximations," *J. Acoust. Soc. Am.* **114**(2), 697–706.
- Freeman, S. E., Buckingham, M. J., Freeman, L. A., Lammers, M. O., and D'Spain, G. L. (2015). "Cross-correlation, triangulation, and curved-wavefront focusing of coral reef sound using a bi-linear hydrophone array," *J. Acoust. Soc. Am.* **137**(1), 30–41.
- Howe, B. M., Worcester, P. F., and Spindel, R. C. (1987). "Ocean acoustic tomography: Mesoscale velocity," *J. Geophys. Res.* **92**(C4), 3785–3805, <https://doi.org/10.1029/JC092iC04p03785>.
- Jensen, F. B., Kuperman, W. A., Porter, M. B., and Schmidt, H. (2011). *Computational Ocean Acoustics* (Springer Science and Business Media, New York), Chap. 5, pp. 337–455.
- Karney, C. (2013). "Algorithms for geodesics," *J. Geod.* **87**, 43–55.
- Kim, J., Park, Y., Lee, S., and Lee, Y. K. (2014). "Underwater glider navigation error compensation using sea current data," *IFAC Proc.* **47**(3), 9661–9666.
- Leonard, J. J., and Bahr, A. (2016). "Autonomous underwater vehicle navigation," in *Springer Handbook of Ocean Engineering*, edited by M. R. Dhanak and N. I. Xiros (Springer, Cham), pp. 341–358.
- McDougall, T. J., and Barker, P. M. (2011). "Getting started with TEOS-10 and the Gibbs Seawater (GSW) Oceanographic Toolbox," http://www.teos-10.org/pubs/gsw/v3_04/pdf/Getting_Started.pdf (Last viewed November 27, 2019).
- Mikhailovsky, P. N., Sagen, H., Worcester, P. F., Baggeroer, A. B., Orcutt, J., Moore, S. E., Lee, C. M., Vigness-Raposa, K. J., Freitag, L., Arrott, M., Atakan, K., Beszczynska-Möller, A., Duda, T. F., Dushaw, B. D., Gascard, J. C., Gavrilov, A. N., Keers, H., Morozov, A. K., Munk, W. H., Rixen, M., Sandven, S., Skarsoulis, E., Stafford, K. M., Vernon, F., and Yuen, M. Y. (2015). "Multipurpose acoustic networks in the integrated Arctic Ocean observing system," *Arctic* **68**, Suppl. 1, 11–27.
- Munk, W., Worcester, P., and Wunsch, C. (2009). *Ocean Acoustic Tomography* (Cambridge University Press, Cambridge, UK), Chap. 5, pp. 173–221.
- Richardson, A., and Nolte, L. (1991). "A posteriori probability source localization in an uncertain sound speed, deep ocean environment," *J. Acoust. Soc. Am.* **89**(5), 2280–2284.
- Saeed, N., Celik, A., Al-Naffouri, T. Y., and Alouini, M.-S. (2019). "Underwater optical wireless communications, networking, and localization: A survey," *Ad Hoc Networks* **94**, 101935.
- Schmidt, H., and Kuperman, W. (1995). "Spectral representations of rough interface reverberation in stratified ocean waveguides," *J. Acoust. Soc. Am.* **97**(4), 2199–2209.
- Skarsoulis, E., and Piperakis, G. (2009). "Use of acoustic navigation signals for simultaneous localization and sound-speed estimation," *J. Acoust. Soc. Am.* **125**(3), 1384–1393.
- Smith, R. N., Pereira, A., Chao, Y., Li, P. P., Caron, D. A., Jones, B. H., and Sukhatme, G. S. (2010). "Autonomous underwater vehicle trajectory design coupled with predictive ocean models: A case study," in *2010 IEEE International Conference on Robotics and Automation*, pp. 4770–4777.
- Tan, H.-P., Diamant, R., Seah, W. K., and Waldmeyer, M. (2011). "A survey of techniques and challenges in underwater localization," *Ocean Eng.* **38**(14–15), 1663–1676.
- Tolstoy, A. (1993). *Matched Field Processing for Underwater Acoustics* (World Scientific Publishing, Singapore), Chap. 4, pp. 91–180.
- Van Uffelen, L. J., Howe, B. M., Nosal, E.-M., Carter, G. S., and Worcester, P. F. (2016). "Localization and subsurface position error estimation of gliders using broadband acoustic signals at long range," *IEEE J. Ocean. Eng.* **41**(3), 501–508.
- Van Uffelen, L. J., Nosal, E.-M., Howe, B. M., Carter, G. S., Worcester, P. F., Dzieciuch, M. A., Heaney, K. D., Campbell, R. L., and Cross, P. S. (2013). "Estimating uncertainty in subsurface glider position using transmissions from fixed acoustic tomography sources," *J. Acoust. Soc. Am.* **134**(4), 3260–3271.
- Worcester, P., Spindel, R., and Howe, B. (1985). "Reciprocal acoustic transmissions: Instrumentation for mesoscale monitoring of ocean currents," *IEEE J. Ocean. Eng.* **10**, 123–137.
- Worcester, P. F., Cornuelle, B. D., Dzieciuch, M. A., Munk, W. H., Howe, B. M., Mercer, J. A., Spindel, R. C., Colosi, J. A., Metzger, K., Birdsall, T. G., and Baggeroer, A. B. (1999). "A test of basin-scale acoustic thermometry using a large-aperture vertical array at 3250-km range in the eastern North Pacific Ocean," *J. Acoust. Soc. Am.* **105**(6), 3185–3201.
- Worcester, P. F., Cornuelle, B. D., Hildebrand, J. A., Hodgkiss, W. S., Jr., Duda, T. F., Boyd, J., Howe, B. M., Mercer, J. A., and Spindel, R. C. (1994). "A comparison of measured and predicted broadband acoustic arrival patterns in travel time-depth coordinates at 1000-km range," *J. Acoust. Soc. Am.* **134**(95), 3118–3128.
- Worcester, P. F., Dzieciuch, M. A., Mercer, J. A., Andrew, R. K., Dushaw, B. D., Baggeroer, A. B., Heaney, K. D., D'Spain, G. L., Colosi, J. A., Stephen, R. A., Kemp, J. N., Howe, B. M., Uffelen, L. J. V., and Wage, K. E. (2013). "The North Pacific Acoustic Laboratory deep-water acoustic propagation experiments in the Philippine Sea," *J. Acoust. Soc. Am.* **134**(4), 3359–3375.
- Zhebel, O., and Eisner, L. (2015). "Simultaneous microseismic event localization and source mechanism determination inversion of location and mechanism," *Geophysics* **80**(1), KS1–KS9.